



Original Paper

Curie Point Depth Estimations for Northwest Iran Through Spectral Analysis of Aeromagnetic Data for Geothermal Resources Exploration

Sina Shirani,¹ Ali Nejati Kalateh,¹ and Younes Noorollahi^{2,3,4}

Received 9 February 2019; accepted 16 October 2019
Published online: 29 October 2019

The northwest of Iran is considered as a promising geothermal zone owing to its geographical properties, tectonic features, and thermal activities, particularly in Sabalan geothermal field. Several large stratovolcanoes such as Sahand and Sabalan mountains in northwestern Iran, each of which has a vast central dome probably located on a tectonic plate, comprising of intrusive and effusive volcanic rocks. This study mainly aimed at performing the spectral analysis of aeromagnetic data to estimate Curie point depth (CPD), geothermal gradient and heat flow in the northwest of Iran using random magnetization (centroid method and forward modeling of the spectral peak method) and fractal magnetization (de-fractal method). The reduced-to-pole aeromagnetic data were divided into 55 overlapping blocks of 80×80 km. The derived range of CPD in the study area using the centroid method, forward modeling spectral peak method and de-fractal method were 9.2–13.9 km, 8.9–13.7 km and 7.2–12.9 km, respectively. The derived values of heat flows in the study area using the above-mentioned methods were higher than 104 mW/m^2 , 105 mW/m^2 and 120 mW/m^2 , respectively. The results of this study were found to have good correlations with wells data and resistivity measurements collected in the Northwest Sabalan geothermal field. Good consistency was also found between the CDPs and earthquake distribution. Moreover, the locations of hot springs and the maximum temperatures of the wells were associated with the variations in the modelled depth of the geothermal resources. Promising regions were in the northeast and southwest parts of the study area.

KEY WORDS: Northwest Iran, Curie point depth estimation, Aeromagnetic data, Geothermal resources.

INTRODUCTION

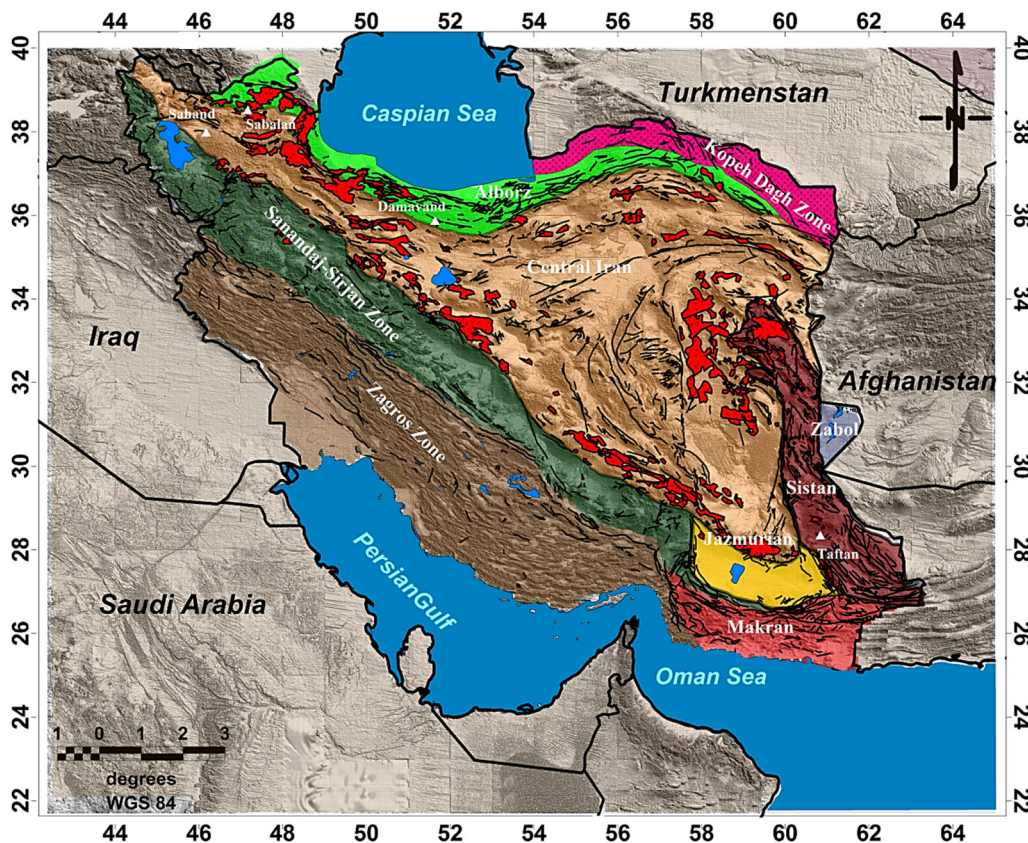
The study area was the northwest of Iran, particularly Sabalan geothermal field, Ardabil province (Fig. 1). Sabalan is a high-enthalpy geothermal field with a water-dominated geothermal system containing several hot springs. Early studies focused on the geological, geochemical and geophysical aspects of this area commenced in 1978 (Fotouhi 1995). Sabalan Mountain is a volcano, located 40 km southwest of Ardebil city and 25 km southeast of

¹Faculty of Mining, Petroleum and Geophysics Engineering, Shahrood University of Technology, Shahrood, Iran.

²Faculty of New Sciences and Technologies, University of Tehran, Tehran, Iran.

³Energy Modelling and Sustainable Energy Systems Research Lab. (METSAP), Faculty of New Sciences and Technologies, University of Tehran, Tehran, Iran.

⁴To whom correspondence should be addressed; e-mail: noorollahi@ut.ac.ir



Legend

- Faults
- Central Iranian Block
- Zagros Zone
- Sanandaj-Sirjan Zone
- Makran Zone
- Tertiary Igneous Rocks
- ▲ Quaternary Volcano
- Alborz
- Quaternary Depressions
- Sistan Structural Zone
- Koppeh Dagh
- Zabol Block

Figure 1. Regional tectonic units of Iran. Modified from the structural map of the National Geoscience Database of Iran, NGDIR; <http://www.ngdir.ir>.

Meshkinshahr city in the northern part of Azerbaijan province. In a study conducted by Bogie et al. (2000), the geological sites of Sabalan were examined carefully and comprehensively. It is also to be noted that the geothermal components are developed from the airborne magnetic anomaly data. In order to investigate regional geothermal exploration, data related to thermal gradient and heat flow values is considered as a representative of subsurface temperature distribution.

The DBMS is regarded as a significant factor for understanding the distribution of temperature in the crust and rheology of the Lithosphere (Ravat

et al. 2007). Moreover, in certain cases, DBMS can be used as an index of the Curie point depth (CPD) estimation of magnetic materials. The CPD temperature, approximately 580 °C, can be considered as an index for the depth to the bottom of the magnetic source. In fact, CPD is the depth at which the magnetic minerals, affected by the high-temperature fluids, lose their magnetic properties and are converted into the paramagnetic state (Tanaka et al. 1999; Porwal et al. 2003; Bansal et al. 2011). CPD provided the information regarding the temperature gradients and heat flow of the crust over the study area.

Since intense seismic activities or natural earthquakes are the result of tectonic activities, it can be argued that the probability of thermal accumulation could be dependent on the observed Curie depths (Aboud et al. 2011). Many studies have been conducted to explore the CPDs of various regions such as east and southeast of Asia (Tanaka et al. 1999), Sinai Peninsula, Egypt (Aboud et al. 2011), and western Turkey (Bilim et al. 2016).

The CPD can be employed to estimate the depths of regional magnetic anomaly. The focus of most regional studies has been on various lithosphere thermal structures in different tectonic settings (Bhattacharyya and Leu 1977; Shuey et al. 1977; Connard et al. 1983; Blakely 1988; Pilkington and Todoeschuck 1993; Fedi et al. 1997; Ross et al. 2006; Porwal et al. 2006; Ravat et al. 2007; Aydin and Oksum 2010; Bansal et al. 2010; Rao et al. 2011; Obande et al. 2014; Salem et al. 2014; Hsieh et al. 2014; Starostenko et al. 2014; Nwankwo and Shehu 2015; Kiyak et al. 2015; Saibi et al. 2015; Bilim et al. 2016; Khojamli et al. 2017; Afshar et al. 2017). These previous studies have considered that many hot springs are found in the northwest of Iran and referring to the geological and geophysical evidence used for evaluating the geothermal prospects. Therefore, this area has high potential for geothermal energy exploration (Noorollahi et al. 2008). Different studies have been conducted to determine the geothermal structures of this area. For instance Khojamli et al. (2016) developed the CPD maps of Maeshkinshahr area in Ardabil Province (N–W of Iran) through considering the random magnetization. They further investigated the bottom depth of the magnetic layer using the centroid method and forward modeling of the spectral peak method. In their study, the appropriate size of magnetic blocks was considered as 100×100 km, with results showing that CPDs varied from 10 to 18.6 km. Khojamli et al. (2017) investigated the depth of magnetic sources in Ardabil province, northwest of Iran, using the de-fractal approach of spectral peak method. As observed in Curie depth map, the Curie depth equaled 7 km in the well NWS8 location of the present study. However, the Curie depth value obtained by Khojamli et al. (2017) equaled 12.4 km in the same location, meaning that well NWS8 was two times higher than (twice the value of) the Curie depth value obtained by the well data. In another study conducted by Amirpour-Asl et al. (2010) a countrywide CPD map was created, and the results

showed that CPDs were varied from 8 to 23 km throughout the country.

In order to discover the geothermal sources and select an optimal site for initial exploration wells, several resistivity structure modeling has been conducted using magneto-telluric (MT) data by the Renewable Energy Organization of Iran (SUNA) (Noorollahi and Itoi 2011; Ghaedrahmati et al. 2013).

In a study by Bromley et al. (2000), an MT survey was conducted through which a very large zone of low resistivity (~ 70 km²) was determined in the study area. Considering the results, obtained from the satellite imagery interpretation, it was concluded that the surficial hydrothermal alteration covered a huge area (~ 10 km²) in the lower elevation part of the project site with low resistivity and overlaid by Quaternary terrace deposits.

Intrusive magmatic bodies are different in terms of density, gravity surveys can be considered as effective tools in geothermal exploration to show the variations of lateral density. Gravity surveys can further be used to show the fracture zones of the geothermal fields (Kiyak et al. 2015; Bédard et al. 2018). It is worth mentioning that about 1000 gravity stations have been utilized with 1.5 km spacing. Two significant high-density areas formed by intrusive (Miocene batholith) or thick lava sequences were demonstrated by the Bouguer anomaly maps. These high-density areas are situated approximately 40 km to the west and 20 km to the northeast side of Sabalan, ostensibly in line with NE trending structures. Moreover, the trachyandesite, belonging to the Eocene epoch, simultaneously occurred with the anomalies of positive gravity. On the other hand, three significant negative residual gravity anomalies were found on the edges of mountain range. Signifying the existence of low-density basins, these anomalies were exactly found within Meshkinshahr reach (to the north), Sarab (to the SW) and Sareyn cities (to the SE). Also observed were certain geological structures formed near the surface, including high-density Quaternary alluvium, sandstone at a deep level along with deeper geological formations such as porous sediments, conglomerate and volcanic tuff.

In another study conducted by Akbar and Fathianpour (2016), the optimizing spectral block dimensions of the aeromagnetic data were used in the Sabalan geothermal field. The CPD was estimated from 5 to 21 km using block dimensions in the range of 10×10 km to 50×50 km.

The main purpose of the current research is to estimate the CPD, geothermal gradient and heat-flow values of subsurface structures in the northwest of Iran, particularly around Sabalan Mountain, using different methods such as centroid depth, de-fractal and forward modeling of the spectral peak. Subsequently, the results obtained from the earthquake data, well information, and hot spring locations were investigated. Generally, a random and uncorrelated distribution of the sources in the aeromagnetic data was assumed in all previous geophysical studies conducted in this area. Since the fractal distribution can change the slope of the Fourier power spectrum of magnetic sources and estimate shallower depths, a correlated fractal distribution of the sources should be taken into consideration to obtain better results.

GEOLOGICAL SETTING

Regional Tectonics

From a tectonic point of view, the study area is affected by a phenomenon similar to the subduction of the Arabian plate under the central Iranian plate (McKenzie 1972). This area is also specified by approximately complex tectonic activities correlated with N-S compressions and E-W spread structures (Rebai and Goffinet 1993).

Sabalan and Sahand volcanoes, known as Quaternary volcanoes, are located within the boundary of these plates in the northwest of Iran. The geological and geophysical features of the study area were explained by Bogie et al. (2000). These regions are categorized into four major stratigraphic units in order of ascending age as follows (Fig. 2):

- Quaternary alluvium, fan and terrace deposits
- Pleistocene post-caldera trachyandesitic flows, domes and lahars
- Pleistocene syn-caldera trachydacitic to trachyandesitic domes, flows, and lahars
- Pliocene pre-caldera trachyandesitic lavas, tuffs, and pyroclastic flow (Khosrawi 2008, p. 1).

Sabalan Mountain is a huge Plio-Quaternary stratovolcano, which presumably erupted in the Late

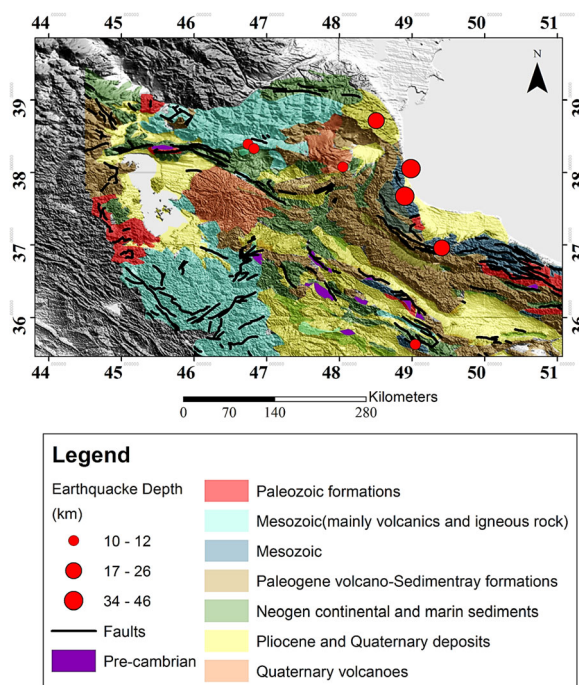


Figure 2. Earthquake distribution on the tectonic map of the study area. Modified after Azad et al. (2011).

Holocene. Caldera collapse caused a sinkage of around 400 m height and 12 km diameter (KML 1998). Over the past decades, the study area has been investigated by different researchers who have considered the fault systems; from a lineation point of view, two types of fault systems are generally characterized in the study area, namely linear faults and arcuate faults. The Sabalan volcano complex, which is located between two main faults from the northwest and southeast, is surrounded by two main NE-SW trends. Almost 50% of the linear structures of this area have in NW-SE directions. Almost 25% of faults have in N-S (the cause of the occurrence of Ghotor-soii in the north of Sabalan), WNW-ESE and WSW-ESE trends. Generally, fracture trend parallel to the main faults in the area. Moreover, two arcuate faults can be recognized around Sabalan volcano. The smaller arcuate fault, situated at the northeast of the mountain, is related to the volcano crater. The absence of this fault in the northwest can be attributed to the high alteration and eruption of the younger lava flows. The larger fault, the

approximate length of which is 14 km, is located in the southwest of Sabalan and observed or interpreted from SPOT satellite imagery (Bromley et al. 2000; Noorollahi et al. 2016).

Geology of Northwest Iran

From a geological perspective and considering the divisions of the northwest of Iran, this area is comprised of two structural parts. The west and southwest parts are the continuum of the Paleozoic platform of central Iran and the west part of Alborz Mountain. This region comprises the Bazgoo, Sahand, Mishno and Marv Mountains in northern Tabriz and the heights in the west part of Jolfa. Apparently, the northeast part of Azarbayejan lacks the Paleozoic platform outcrop, which can be found in other parts of Iran. Instead, this area is covered with the Mesozoic Flieship outcrop. Some parts of this region, which include the sedimentary basin of Moghan plain and Ahar and Kharvana heights, are also covered with the tertiary sedimentary outcrops with unique features. The Paleozoic rocks are mostly of sedimentary and internal igneous types, which can be observed in almost all mountains of this area, such as Mishoodaghi, Marvdaghi, and Sufiyan and some northern parts of Marand city. The Mesozoic rocks are mostly of sedimentary type. During the Cenozoic period, the rocks were mostly igneous (intrusive and especially extrusive) and pyroclastic such as tuffs and volcanic breccia, all of which have still extensively covered this area which is also comprised of volcanic rocks and intrusive bodies, serving as the main characteristic of geothermal energy potential, particularly those belonging to Eocene to Miocene periods (Fig. 3).

The tectonic effects along with the formation of the giant volcanos (Sabalan and Sahand) at the end of the Tertiary and Quaternary periods are known as the main features of this area. The basalt lava, extruded from the large Ararat volcano in Turkey and covering certain parts of northwest plains in Maku-Azarbayjan, can be considered as an evidence of the last volcanic activities in this region. Sahand peak, with 3814 m height, is considered as the highest part of this area. The lowest part (50 m above sea level) is known as the sedimentary basin of Moghan Plain, belonging to Kura-Aras land which is probably the remains of the sedimentary basin of Tethys Ocean. Tabriz fault is the main fault in this area, composed of several other faults. The last movement of this

fault was dextral (right-handed movement), progressing 111 km from south of Abhar to Ararat mountain. The movements and displacements of this fault impacted the Plougha-Quaternary volcanic eruptions of Sahand Mountain resulting in the formation of Bostan-abad hot springs (Fig. 4).

METHODOLOGY

The mathematical formulas of these methods are mainly based on the layers' flatness with the distribution of magnetization, called random (uncorrelated) magnetization models or self-similar (fractal) magnetization models. The conventional methods used for CPD estimation are based on the random and uncorrelated dispersion of the magnetic sources, equivalent to the white noise distribution. According to the boreholes information, the distribution of magnetic sources is regarded as a combination of fractal and random dispersion of magnetic sources themed as "scaling distribution" (Maus and Dimri 1995; Bansal et al. 2010, 2011).

Random Magnetization

According to random magnetization, two approaches are generally applied to estimate the depth to the bottom of magnetic sources: (a) the spectral peak method, initially presented by Spector and Grant (1970) and applied by Shuey et al. (1977), Blakely (1988) and Salem et al. (2000) and (b) centroid method, primarily established by Bhat-tacharyya and Leu (1977) and later developed by Okubo et al. (1985) and Tanaka et al. (1999) It should be noted that an initial estimate of the depth to the top of the magnetized layer is required in both methods (Salem et al. 2014).

Centroid Method and Heat Flow

After transferring the spatial data to the frequency domain, a correlation is established by these methods between the magnetic anomalies spectrum and magnetic sources depth (Tanaka et al. 1999; Shuey et al. 1977; Waples 2002). Since these methods cannot simultaneously estimate the depth to the bottom and top of magnetic resources, a primary estimation is required for the depth to the top of the resources. However, in a study conducted by Shuey

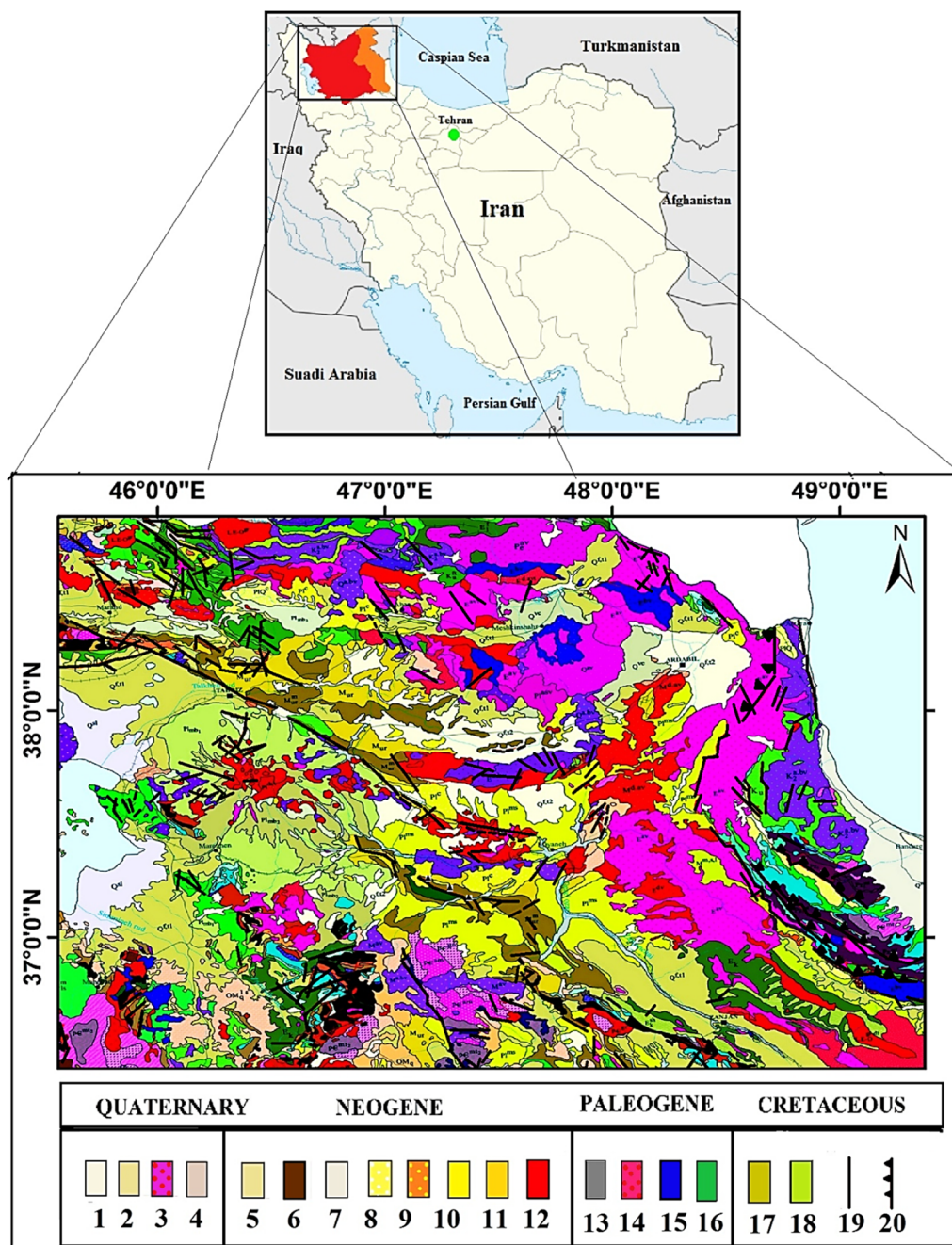


Figure 3. Geological map of the study area in Northwest of Iran. 1 = Salt Lake fan. 2 = High-level pediment fan. 3 = Andesitics Volcanics. 4 = Volcanogenic Conglomerate. 5 = Basaltic Volcanics. 6 = Mudstone. 7 = Pyroclastics. 8 = Ash Flow. 9 = Sandstone and Mudstone. 10 = Dacitic subvolcanic rocks. 11 = Pale-yellow to red sandstone. 12 = Light-red to brown marl. 13 = Andesitic Volcanics. 14 = Basaltic volcanic rocks. 15 = Dacite to andesitic volcanic rocks. 16 = Siltstone and sandstone. 17 = Low-level pediment. 18 = Pyroclastic and claystone. 19 = Major fault in general. 20 = Minor fault in general.

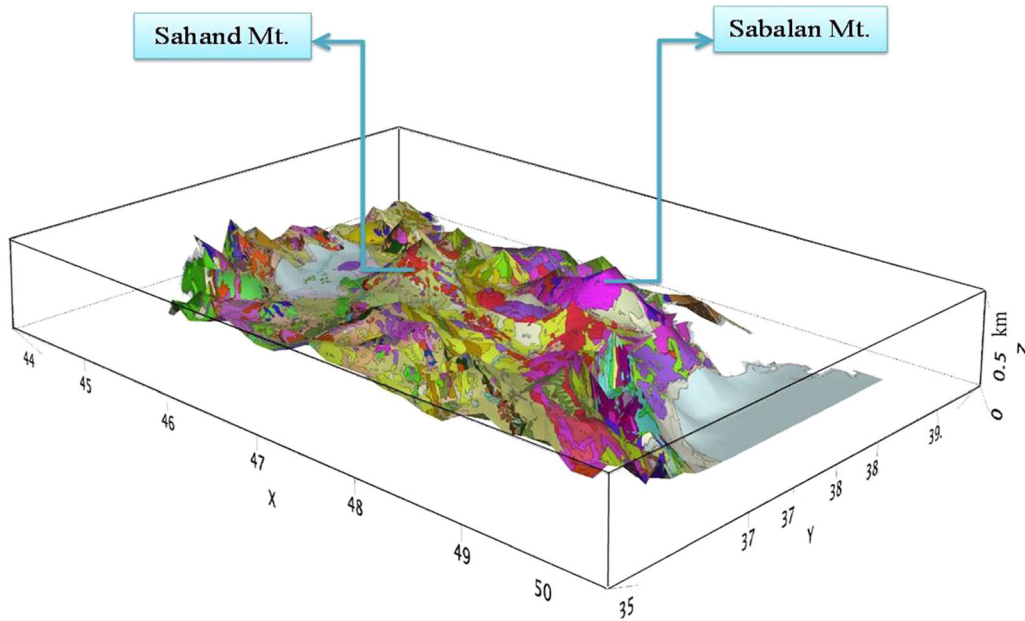


Figure 4. 3D topographic map overlaid by a geological map of Northwest of Iran.

et al. (1977), it was demonstrated that the centroid method was more efficient in estimating the depth of regional magnetic anomalies.

The formula and theory of “the power spectral density (PSD) of the observed magnetic field ($\varphi_{\Delta T} = (k_x, k_y)$)” is derived from Blakely (1996) as follows:

$$P(k_x, k_y) = \varphi_M(k_x, k_y) \times F(k_x, k_y) \quad (1)$$

$$F(k_x, k_y) = 4\pi^2 C_m^2 \phi(k_x, k_y) |\Theta_m|^2 |\Theta_f|^2 e^{-2|k|Z_t} \times (1 - e^{-|k|(Z_b - Z_t)})^2 \quad (2)$$

where (k_x, k_y) are known as wave numbers in directions of “ x, y ”, φ_M is the magnetization power spectrum, and C_m^2 is a constant quantity. $|\Theta_m|^2$ and $|\Theta_f|^2$ represent factors of magnetization and magnetic field directions, respectively. Moreover, Z_t, Z_b are considered as the top-depth and bottom-depth of magnetic layers, respectively. Given the random magnetization $M(x, y)$, there is a random function in terms of x and y ; accordingly $\varphi_M(k_x, k_y)$ becomes a constant quantity. The radially averaged power spectrum (RAPS) equals (Stampolidis et al. 2005):

$$P(k) = A_1 e^{-2|k|Z_t} (1 - e^{-|k|(Z_b - Z_t)})^2 \quad (3)$$

where A is considered as a constant quantity and k is the indicator of the wave number.

Considering the power spectrum, derived from a low wave number, the central depth of magnetic resource can be more simply calculated as follows (Bhattacharyya and Leu 1977; Okubo et al. 1985; Aydın, and Oksum 2010):

$$\ln\left(\frac{P(k)^{\frac{1}{2}}}{k}\right) = A_2 - |k|Z_0 \quad (4)$$

$$\ln(P(k)^{\frac{1}{2}}) = A_3 - 2|k|Z_t \quad (5)$$

where P is the power spectral density (PSD), and A_2 and A_3 are constant quantities. After obtaining Z_t, Z_0 , the bottom-depth of the resources can be calculated as (Okubo et al. 1985; Tanaka et al. 1999):

$$Z_b = 2Z_0 - Z_t \quad (6)$$

Moreover, Eq. 7, which indicates the Fourier’s law, can be used to establish a connection between the geothermal gradient and heat flow thus (Tanaka et al. 1999; Stampolidis et al. 2005; Maden 2010):

$$q = k \frac{\partial T}{\partial Z} \quad (7)$$

where k is thermal conductivity and q is considered as the heat flow.

It should be noted that DBMS does not directly indicate the CPD in many cases. Additionally, in certain cases, the bottom of magnetic sources may

be a lithological contact corresponding to the base of the crust and not the actual CPD; additionally, there might be artifacts associated with the acquisition of the data.

$$\theta_c = \left(\frac{\partial T}{\partial Z} \right) Z_b \quad (8)$$

where Z_b and θ_c are the CPD and the Curie temperature, respectively. If there is no thermal source between the Curie point and the earth surface, thermal gradient is considered as a constant quantity (Fig. 5).

Forward Modeling of the Spectral Peak

As a new approach, the method of forward modeling (iterative matching) of the spectral peak was proposed by Finn and Ravat (2004), and Ravat et al. (2007) to improve simultaneously the bottom

and top-depth estimation of the magnetic sources using the following formula:

$$P(k) = C(e^{-|k|Z_t} - e^{-|k|Z_b})^2 \quad (9)$$

where P is power spectrum and k is wave number.

An appropriate model can be obtained between the observed peak and the first model based on Eq. 9 via a constant quantity parameter called “ C ”, comprising the depth-independent parameters. The constant C should be modified to assist the modeled curve moving up and down and create a proper fitting for the observed peak. The curve’s slope is controlled by Z_t at high wave numbers. Moreover, the spectral peak location is controlled by Z_b at short wave numbers relative to wave number axis. Therefore, the combination of both Z_t and Z_b is employed to control the adjacent slope around the spectral peak. The bottom and top-depth of the magnetic sources are simultaneously estimated using Eq. 9, which is considered as the main advantage of this method (Ravat et al. 2007).

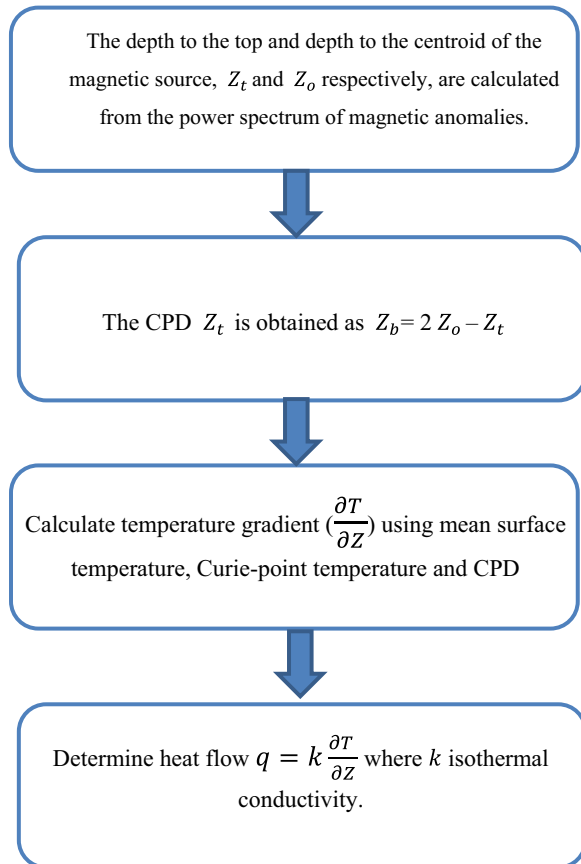


Figure 5. The flow-chart showing the procedure used in the heat calculation (Obande et al. 2014).

Fractal Magnetization

As mentioned by Fedi et al. (1997) the Spector & Grant (1970) equation has an essential power-law form by the large random variation of the source:

$$P(k) = Ak^{-\beta} \quad (10)$$

where P , k are indicators of the power spectrum, wavenumber, respectively. A is a constant quantity and β shows the scaling factor, the self-similarity degree of the magnetization, which is dependent on the geological features and lithology of the area and varies over different regions. The values of β (i.e., the slope of the spectrum in log–log scale) represent the degree of correlation. Therefore, a larger β is the stronger is the long range correlation (Pilkington and Todoeschuck 1993; Maus and Dimri 1994; Fedi et al. 1997; Bansal and Dimri 1999, 2001; Dimri et al. 2003; Bansal et al. 2006, 2016).

Based on these assumptions, three unknown parameters, namely “ Z_t , ΔZ and β ”, representing depth to the top of magnetic layers, thickness of the magnetic layers and scaling factor, respectively, are utilized to completely describe the theoretical power spectrum caused by the slab of fractal magnetization distribution (Maus et al. 1997):

$$\begin{aligned} \Phi_{B1D}(k_H)d\theta &= C - 2k_H Z_t - k_H \Delta Z - \beta \ln(k_H) \\ &+ \ln \left[\int_0^\infty (\cosh(k_H \Delta Z) - \cos(k_z \Delta Z)) \left(1 + \left(\frac{k_z}{k_H} \right)^2 \right)^{-1-\frac{\beta}{2}} dk_z \right] \end{aligned} \quad (11)$$

where C is the constant and the adjustment of geomagnetic field appears exclusively in the constant parameter “ C ” angle with respect to k_x , $k_H = |k_H|$ represents the wave number norm in the horizontal plane, which equals $k_H = (k_x, k_y)$, θ is considered as the angle relative to k_x , and β represents the scaling factor that describes the magnetization fractal degree. For example, $\beta = 0$ is the random magnetization model, explained by Spector and Grant (1970), and restated in Bouligand et al. (2009), $\beta > 0$ values are indicators of increasingly correlated magnetic susceptibility in the depth, and $\beta < 0$ shows the anti-correlated magnetic susceptibility in the depth. With the increase in the magnetization fractal parameter, the slopes of the power spectrum increase. The lower value of the fractal parameter entails an error in the estimation of the bottom and top depth.

De-fractal Method

The idea behind the de-fractal method is that the observed power spectrum can be represented through the power spectrum of the fractal magnetization through considering the fact that the magnetization has a fractal behavior in the horizontal plane (x and y directions) and is constant in the (Z) direction. Accordingly, the observed power spectrum equals the multiplication of the power spectrum of random magnetization and $k^{-\alpha}$ as follows (Salem et al. 2014):

$$P_F(k_x, k_y) = P_R(k_x, k_y) * k^{-\alpha} \quad (12)$$

where $P_F(k_x, k_y)$ is the observed power spectrum. The power spectrum derived from the distribution of uncorrelated magnetization is also illustrated by $P_R(k_x, k_y)$. k is the radial wave number and α is the fractal index of $\alpha = \beta - 1$, in which β is referred to as the fractal parameter of magnetization (Maus and Dimri. 1994). If α is obtained, the de-fractal process can be implemented on the observed spectrum through the multiplication of k^α factor and the observed spectrum. Thus, a power spectrum can be

extracted corresponding to the random magnetization, as:

$$P_R(k_x, k_y) = P_F(k_x, k_y)k^\alpha \quad (13)$$

The obtained spectrum can be regarded as a random magnetization via eliminating the fractal effect, a technique employed to modify the power spectrum magnetic field of the fractal magnetization distribution (Salem et al. 2014). The Centroid technique along with the forward modeling of the spectral peak is further utilized in de-fractal method. Power spectrum correction is not a novel perception, hence the fact that Fedi et al. (1997) and Ravat et al. (2007) calculated the top depth of the magnetic layer from a corrected power spectrum using the same method and suggested a modified centroid method. In their study, the power spectrum was corrected to modify the scaled power spectrum. They further proposed that the new method had many advantages over the conventional centroid method.

In previous studies where conventional methods were used, the data was (were) filtered prior to estimating the depth, and the number of points related to the high wave numbers was eliminated. Therefore, CPD was estimated deeper than the real depth. The advantage of the modified method is that it is not required that data are filtered before depth estimation.

Although the power spectrum becomes de-fractal by considering various amounts of α , the exact quantity is selected through fitting the modeled power spectrum, obtained from the forward-modeling of the spectral peak to the de-fractal spectrum. Figure 6 shows the de-fractal method, used for estimating the bottom depth of magnetic anomalies. A small amount of α is selected at the beginning of the process. The whole process, executed on the observed spectrum, is shown in the flowchart. The centroid method is used to estimate the top-depth and center-depth of magnetic layers. The validity of the fitting process can be evaluated, visually, but this study mainly focuses on the fitting process of the highest wavelengths, while ignoring the local fluctuations of power spectrum's curve.

DATA PROCESSING AND ANALYSIS

The aeromagnetic survey of Iran, covering the study area, was conducted by the Aero Service Company (Houston, Texas) and was recorded dur-

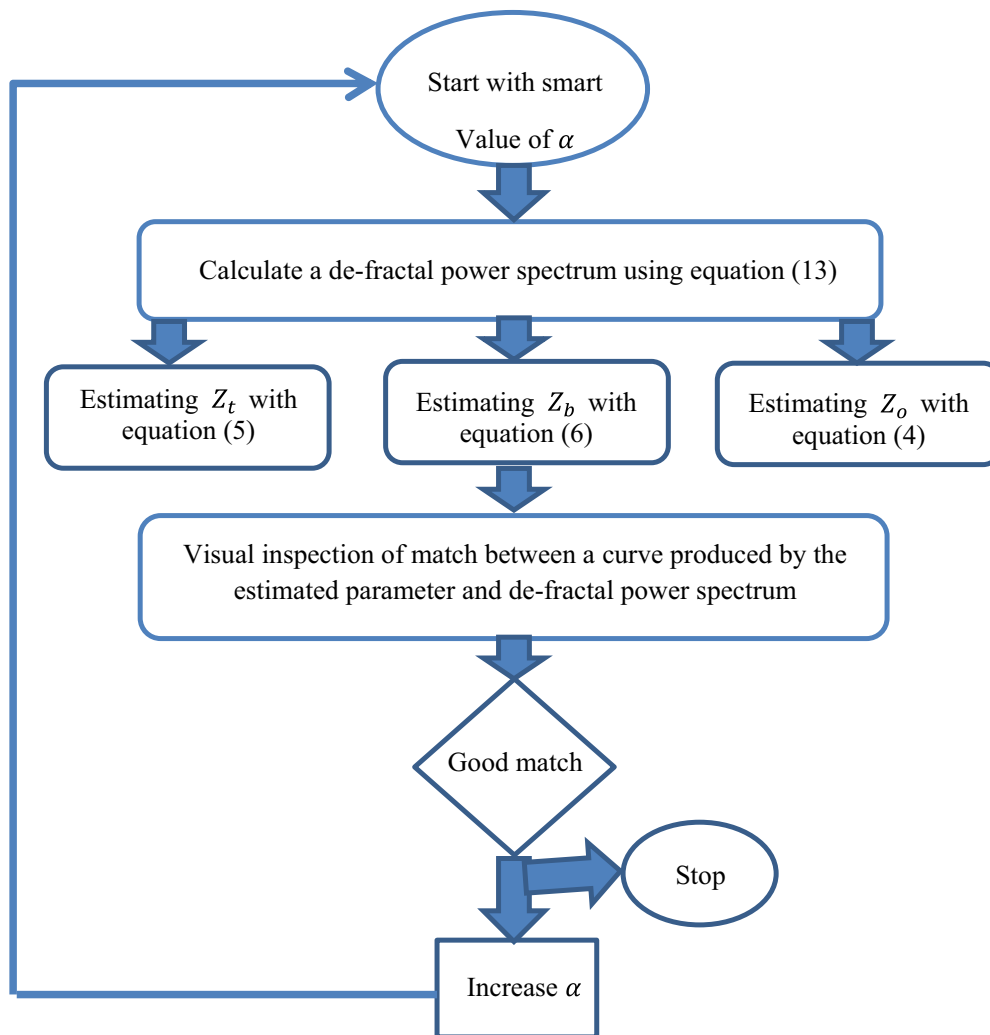


Figure 6. The de-fractal approach flowchart, used for the estimation of the Bottom depth of the magnetic layer (after Salem et al. 2014).

ing 1974–1977. The survey was performed along a set of lines in the north–south direction with 7.5 km spacing. The average spacing of control flight lines was considered 40 km and the average flight elevation was selected 500 m above the ground level. The regional correction was performed based on the International Geomagnetic Reference Field (IGRF1976) to produce a corrected magnetic anomaly map (Fig. 7). Magnetic inclination is considered as one of the factors affecting the shape of magnetic anomaly, the angle of which is considered 90° in both magnetic poles and zero in the equator. In other areas, the inclination angle ranges from zero to 90 degrees. All magnetic anomalies are asymmetric in shape except for the anomalies

caused by the mass at both magnetic poles. Reduction to pole converts the asymmetry of the anomaly into a symmetric shape, hence the conversion of the magnetic anomaly into the anomaly, measured in magnetic poles. This helps precisely characterize the location of anomaly on the anomaly sources. Moreover, in the study area, the declination and inclination angles values were in the range of (3.6° – 4.1°) and (54.3° – 56.4°), respectively. Primarily, RTP transformation was conducted and this map was prepared. In the next step, the power spectrum of each block was computed using the fast Fourier transform (FFT).

It is important to determine the dimensions of the blocks as they directly affect the magnetic con-

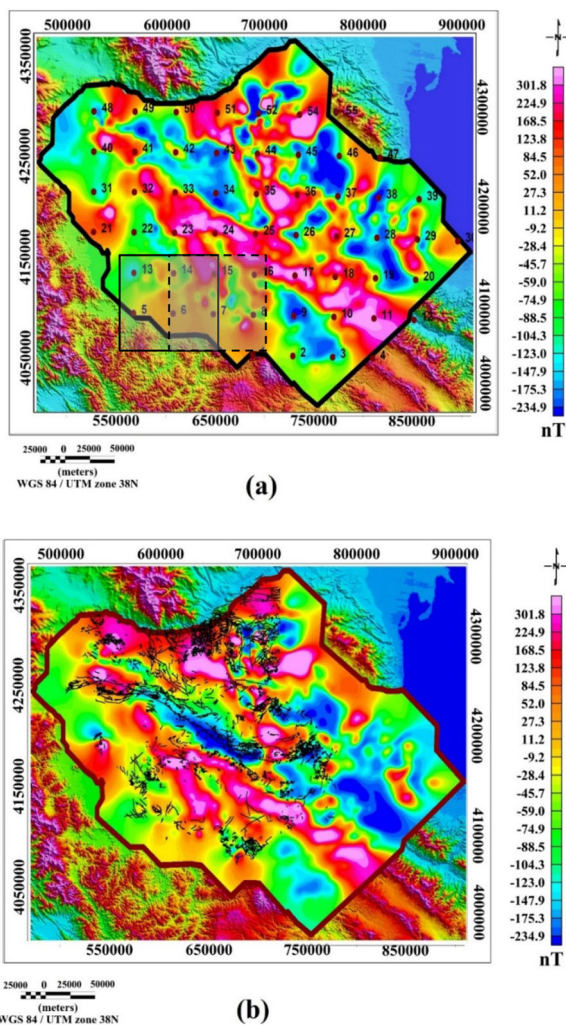


Figure 7. (a) Selection of overlapping blocks on the RTP map. Solid circles are indicators of the centers of blocks (named as 1–55); (b) RTP map of the study area (the black thin lines indicate the fault).

tent and any approachable depth of the block. Bigger block sizes provide the possibility to detect longer wavelengths in relation to deeper magnetic sources. However, block sizes should also be small enough to prevent the influences of spectra, which result from the adjacent magnetic bodies. In a study conducted by Trifonova et al. (2009), the depth of the Curie point was examined using an optimal block size not interrupting the peak of the spectrum. East and Southeast of Asia were divided into sub-regions (approximately 200 × 200 km) based on magnetic or aeromagnetic data by Tanaka et al. (1999). Blakely (1988) divided the Nevada area into blocks (120 km × 120 km) and mapped the curie

depth of Nevada state Connard et al. (1983) conducted a magnetic survey in Cascade Range (central Oregon); subdividing the study area into overlapping magnetic blocks (77 × 77 km) and obtaining radially average power spectrum for each block. If the source of magnetic bodies is deeper than $L/2\pi$, a proper response cannot probably be achieved by spectral methods (Shuey et al. 1977). In the present study, the RTP map was divided into 55 blocks with 80 × 80 km dimensions, and 50% overlapping was considered for adjacent blocks. As seen in Figure 7, the CPD was attributed to the center of each block for all blocks.

The 2D radially average power spectrum of aeromagnetic data was calculated for each block using a model developed in MATLAB via FFT method. Figure 8 shows that the CPDs of each block were calculated using the graph plotting spectrum against the wavenumber (radians per km). Shallow earthquakes mostly occurred in areas with shallow CDPs.

RESULTS OF CPD ESTIMATION

Centroid Method

Logarithmic graphs of the power spectral density against wavenumbers were procured for each block. The plots of blocks 8, 23 and 44 are shown in Figure 9. Equations 4 and 5 can be further used along with LS (least-square) method to obtain the depths to the top and centroid of the available magnetic layer through fitting the certain parts of the power spectrum graph with high and low wavenumbers. Thus, Eq. 6 was utilized to calculate DBMS and CDP. A flight elevation of 0.5 km was subtracted from CPDs. Because in the calculation of CPD estimation assumed that the data is taken from the earth surface, therefore subtract the flight elevation from the obtained results for CPD. As shown in Table 1, the depths were obtained from ground level. Figure 10 illustrates the location of hot springs in the NW of Iran along with the CDP map.

Considering Figure 2, since some earthquakes have occurred in the study area, it can be argued that earthquakes can be the main reason for the existence of thermal amassing which can also be associated with CPD. The heat flow map of the study area is shown in Figure 11, in which the area with lower heat flow value ($\sim 104.3 \text{ mW/m}^2$) is situated in block 24, while the area with the highest heat flow

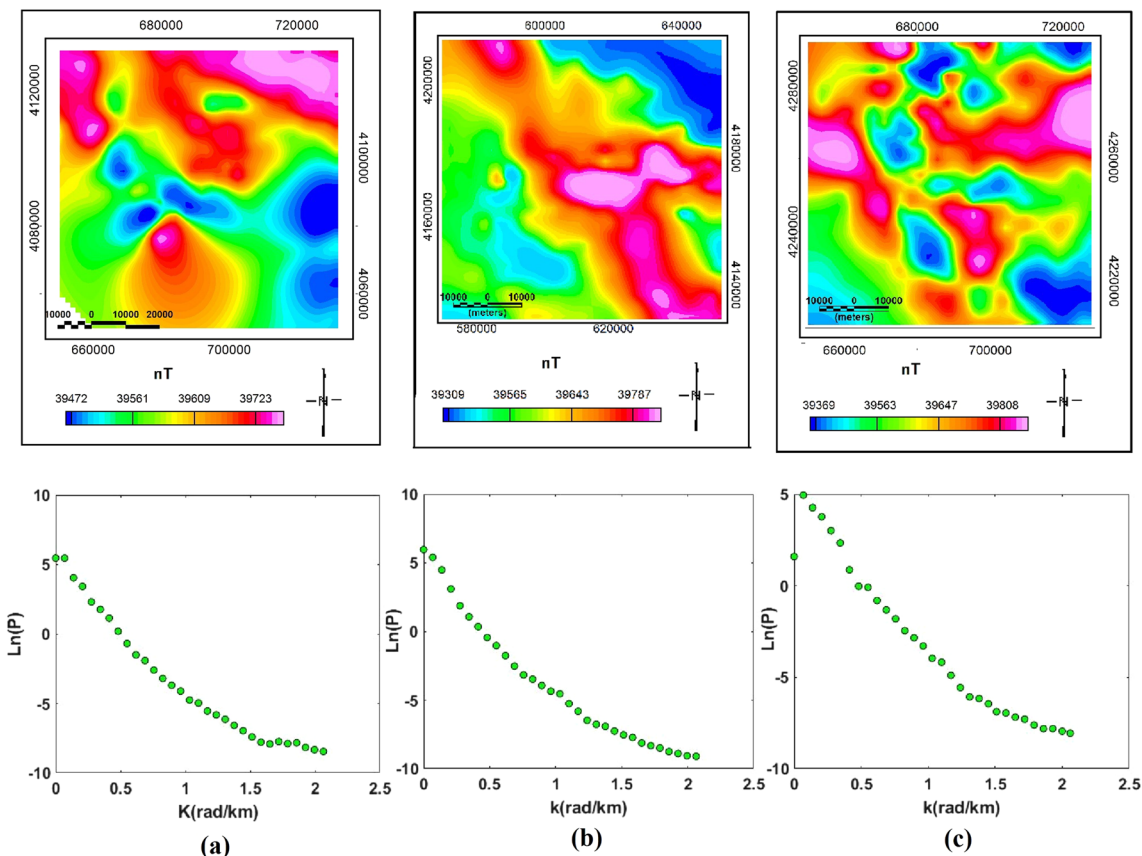


Figure 8. Power spectrum plot, calculated from RTP map for (a) block 8; (b) Power spectrum plot for block 23; (c) Power spectrum plot for block 44.

value ($\sim 159.3 \text{ mW/m}^2$) is located in block 38. The geothermal gradient estimation is shown in Figure 12 and calculated based on Eq. 8 through considering the curie-temperature of magnetite ($HC = 580 \text{ }^\circ\text{C}$) and the thermal conductivity ($k = 2.5 \text{ W/m}^\circ\text{C}$) for igneous bodies. Nevertheless, in this study, the geothermal gradient values were calculated in the range of 41.7 and 57.4 $^\circ\text{C/km}$ (Fig. 12).

Forward Modeling of the Spectral Peak

CPDs obtained by the spectral peak forward modeling method are shown in Figure 13 and Table 2. As is observed in Figure 14, the green scatters represent the Fourier spectrum, while the red curve indicates the modeled spectrum generated using assumed Z_b , Z_t values in Eq. 9. Consequently, the top and bottom depths of the magnetic layer were calculated considering the forward modeling spec-

tral peak method and using Eq. 9. In some cases, the forward modeled spectra are not properly correlated with the observed spectra. In order to achieve the most optimal match, the possibility of fitting process iteration was provided between the observed and modeled data via forward modeling. The results were accepted or rejected based on the fitting of the modeled spectra and the observed data. The forward modeling can be performed to determine or estimate the ‘minimum depth in the absence of spectral peak’. In this study, the spectral peaks appeared by the selection of the optimal dimension for each block ($80 \times 80 \text{ km.}$). The results of the CPDs, calculated by forward modeling of the spectral peak, varied from 8.9 to 13.7 km. Considering the obtained CPDs, the geothermal gradient map of the study region (Fig. 15) was produced using forward modeling, which indicated that the high geothermal gradient contours were mostly centered around Sabalan Mountain to the east of Ardabil city and around Kharajo area. This quantity varied from 42.3

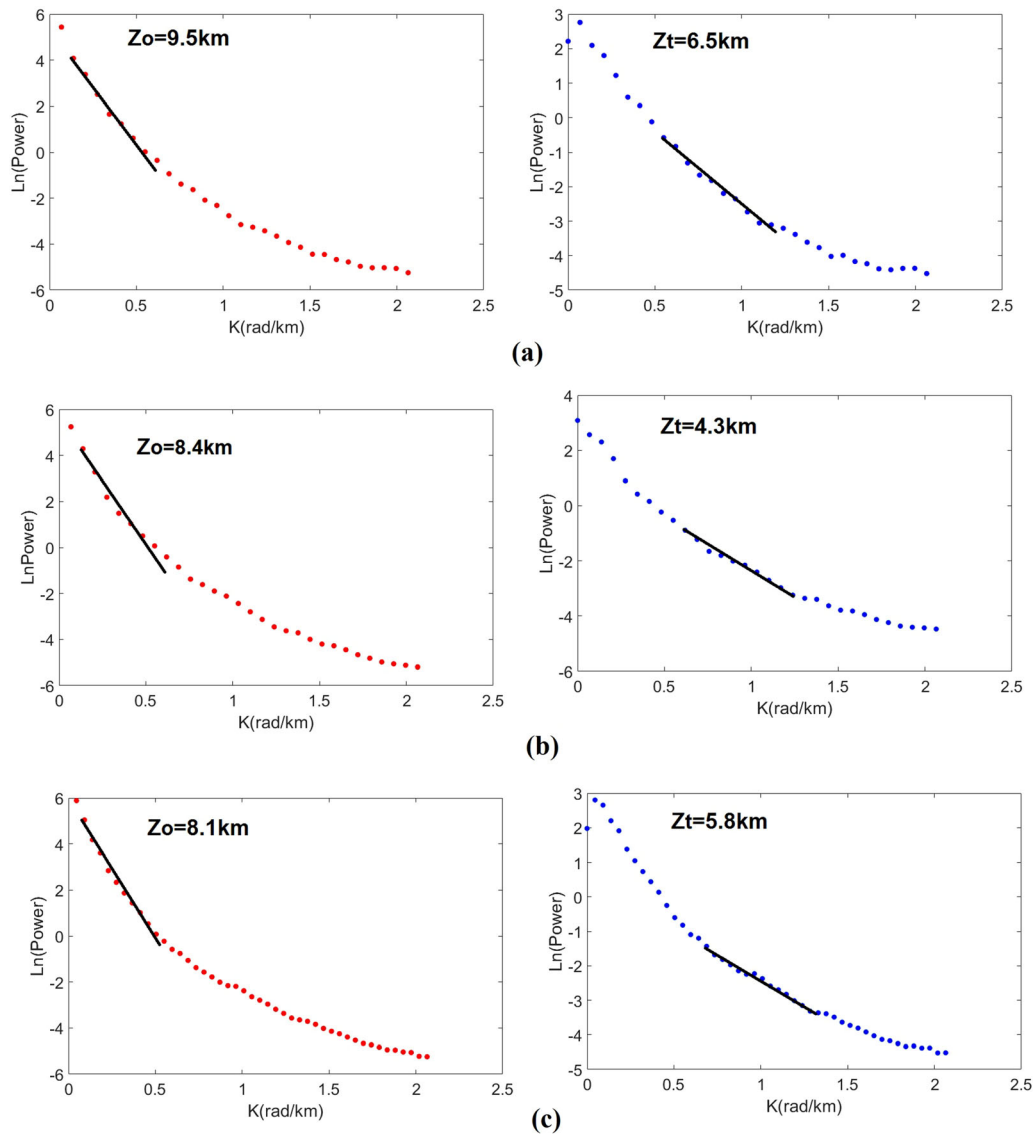


Figure 9. Spectral analysis for (a) block 8, (b) block 23, (c) block 44, based on the RTP aeromagnetic map. Spectra calculated from Eq. 2 to estimate depth to the centroid, Z_0 (Red curve) and spectra calculated from Eq. 4 to estimate depth to Z_t (Blue curve), Solid lines represent the least-square fit of the power spectra.

to $63.7\text{ }^\circ\text{C/km}$ over different regions. The heat flow map of the study area was produced using Eq. 7. The results revealed that the heat flow values were in the range of $105.8\text{--}159.3\text{ mW/m}^2$. The results further revealed that the heat flow value was significantly dependent on geological features. Generally, the units with high heat flow values belonged to the volcanic and metamorphic units. Furthermore, the tectonic activities of the different regions were significantly affected by the heat flow (Tanaka et al.

1999). For instance, the main faults were mostly located within the border of regions situated between low and high CPD (Fig. 13).

De-fractal Method

After conducting the initial data processing, the de-fractal approach was applied to the power spectrum of each block based on different α values. The

Table 1. Estimated CPD, geothermal gradients, and heat flow by applying the centroid depth method for the 55 blocks in the study area

Block number	Coordinates (UTM)		Z_t (km)	Z_0 (km)	CPD (km)	Geothermal gradient ($^{\circ}\text{C}/\text{km}$)	Heat flow (mW/m^2)
	Easting (km)	Northing (km)					
1	689,950.3	4,050,000	6.0	9.8	13.6	42.6	106.6
2	729,950.3	4,050,000	5.1	8.3	11.5	50.4	126.1
3	769,950.3	4,050,000	3.5	5.6	10.6	54.7	136.8
4	809,950.3	4,050,000	3.5	6.2	11.3	51.3	128.3
5	569,950.3	4,090,000	5.8	7.8	11.9	48.7	121.8
6	609,950.3	4,090,000	5.9	10.1	10.2	56.9	142.2
7	649,950.3	4,090,000	5.0	9.4	13.8	42.0	105.1
8	689,950.3	4,090,000	6.5	9.5	12.5	46.4	116.0
9	729,950.3	4,090,000	6.0	9.0	12.0	48.3	120.8
10	769,950.3	4,090,000	5.9	9.1	12.3	47.2	117.9
11	809,950.3	4,090,000	4.2	6.7	11.9	48.7	121.8
12	849,950.3	4,090,000	7.6	11.8	16.0	36.3	90.6
13	569,950.3	4,130,000	6.3	10.2	9.1	63.7	159.3
14	609,950.3	4,130,000	6.3	10.4	9.6	60.4	151.0
15	649,950.3	4,130,000	7.2	10.8	14.4	40.3	100.7
16	689,950.3	4,130,000	6.8	10.2	13.6	42.6	106.6
17	729,950.3	4,130,000	8.2	12.1	16.0	36.3	90.6
18	769,950.3	4,130,000	3.7	8.0	12.3	47.2	117.9
19	809,950.3	4,130,000	5.1	9.0	12.9	45.0	112.4
20	849,950.3	4,130,000	5.2	9.5	13.8	42.0	105.1
21	529,950.3	4,170,000	5.3	7.9	9.8	59.2	148.0
22	569,950.3	4,170,000	4.0	6.5	9.3	62.4	155.9
23	609,950.3	4,170,000	4.3	8.4	12.5	46.4	116.0
24	649,950.3	4,170,000	8.2	12.6	17.0	34.1	85.3
25	689,950.3	4,170,000	6.7	10.6	14.5	40.0	100.0
26	729,950.3	4,170,000	8.4	12.5	16.6	34.9	87.3
27	769,950.3	4,170,000	5.9	8.1	12.9	45.0	112.4
28	809,950.3	4,170,000	4.8	7.2	13.1	44.3	110.7
29	849,950.3	4,170,000	4.8	8.7	12.6	46.0	115.1
30	889,950.3	4,170,000	4.0	6.8	13.1	44.3	110.7
31	529,950.3	4,210,000	5.3	9.1	12.9	45.0	112.4
32	569,950.3	4,210,000	4.0	7.1	12.6	46.0	115.1
33	609,950.3	4,210,000	4.5	7.3	11.9	48.7	121.8
34	649,950.3	4,210,000	6.0	8.3	13.1	44.3	110.7
35	689,950.3	4,210,000	5.8	8.2	12.1	47.9	119.8
36	729,950.3	4,210,000	6.0	8.3	9.9	58.6	146.5
37	769,950.3	4,210,000	2.5	5.1	7.7	75.3	188.3
38	809,950.3	4,210,000	4.2	6.2	11.9	48.7	121.8
39	849,950.3	4,210,000	4.1	6.9	12.1	47.9	119.8
40	529,950.3	4,250,000	4.8	8.4	12.0	48.3	120.8
41	569,950.3	4,250,000	5.0	9.0	13.0	44.6	111.5
42	609,950.3	4,250,000	5.2	9.1	13.0	44.6	111.5
43	649,950.3	4,250,000	5.8	9.8	13.8	42.0	105.1
44	689,950.3	4,250,000	5.8	8.1	10.4	55.8	139.4
45	729,950.3	4,250,000	5.0	7.4	9.8	59.2	148.0
46	769,950.3	4,250,000	4.0	6.6	9.2	63.0	157.6
47	809,950.3	4,250,000	5.3	8.5	11.7	49.6	123.9
48	849,950.3	4,250,000	5.3	9.4	13.5	43.0	107.4
49	529,950.3	4,290,000	4.7	8.7	10.7	54.2	135.5
50	569,950.3	4,290,000	5.7	10.0	11.1	52.3	130.6
51	609,950.3	4,290,000	6.0	10.0	10.3	56.3	140.8
52	649,950.3	4,290,000	3.0	6.3	9.6	60.4	151.0
53	689,950.3	4,290,000	4.5	6.8	9.1	63.7	159.3
54	729,950.3	4,290,000	4.2	6.6	9.0	64.4	161.1
55	769,950.3	4,290,000	4.8	8.4	12.0	48.3	120.8

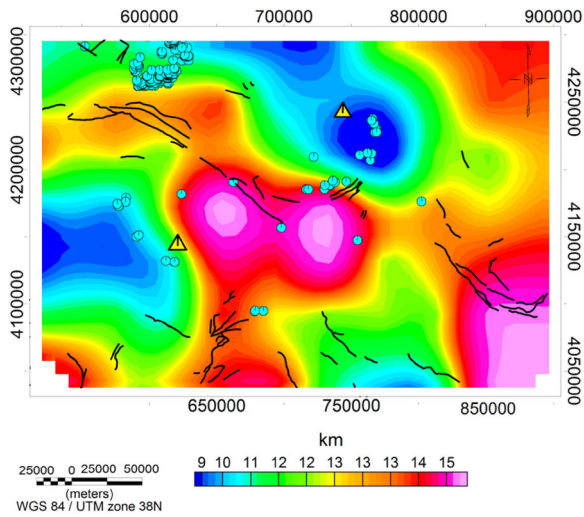


Figure 10. CPD map (Centroid method), and the faults of the study area. Yellow triangle shows the location of the Sabalan Mountain and Sahand Mountain and the blue circles are indicators of hot springs.

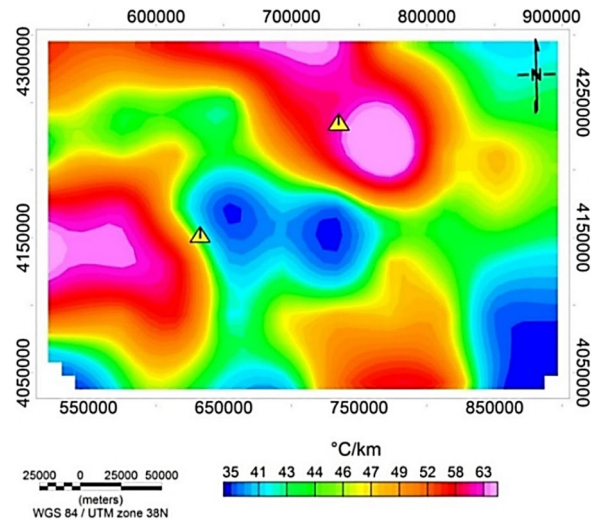


Figure 12. Geothermal gradient map (Centroid method) in the study area.

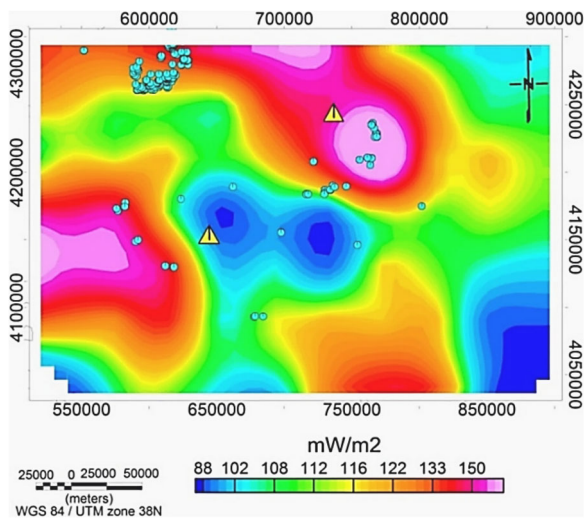


Figure 11. Heat flow map (Centroid method) of the study area. Yellow triangles show the location of the Sabalan Mountain and Sahand Mountain and blue circles show hot springs.

CPD estimation of Z_b and Z_t of the magnetic layer within the blocks is explained in the flowchart in Figure 6. It is highly important to select the most appropriate wavelength band in calculating the centroid and top of the deepest anomaly sources.

The process is relatively dependent on a researcher’s perspective. For example, fitting a straight line in the logarithm plot of the power spectrum

against wave number is considered as a subjective trend (Fig. 16).

Two types of blocks were found in this study. In the first type, a suitable wavelength was easily determined owing to the linear display in the spectra’s plot. However, the selection of the wavelength band was highly difficult in the second type of blocks. Nevertheless, the wavelength was selected through searching for a nearly straight line in the plots to compute the centroid and the top depth. An example of the de-fractal approach for block 40 is shown in Figure 17 which demonstrates the process of obtaining α values, ranging from 1 to 3.3, based on the best possible fitting between the modeled power spectrum and de-fractal spectrum. Different values of α were obtained in the study area, probably due to the existence of different magnetic features of the rocks.

The values of Z_b and Z_t for each de-fractal power spectrum were obtained using Eqs. 4, 5, and 6, while the magnetic bottom depths ranged from 7.2 to 12.9 km (Fig. 18). The appropriate fractal value, selected by acceptable fitting, indicated the fitting process between the modeled power spectrum and the de-fractal spectrum. The value of α was continuously raised until a suitable matching is obtained. Table 3 shows the estimated values of the depth to the top and bottom of the magnetic sources along with fractal parameter α of the study area.

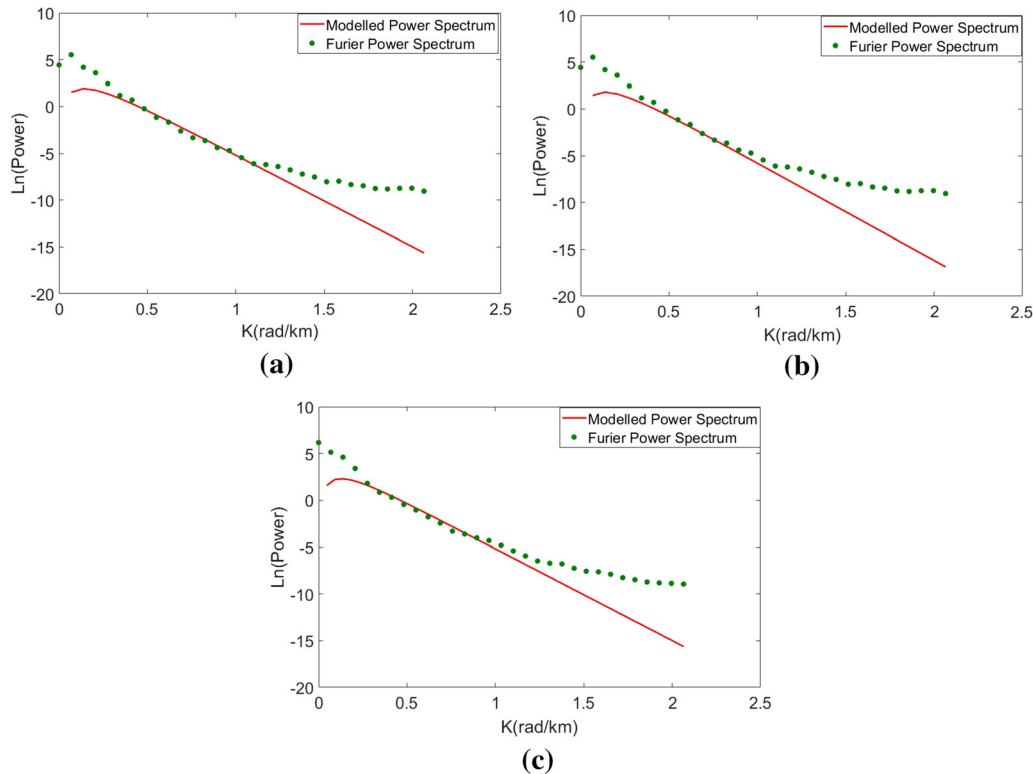


Figure 13. CPD map (forward modeling of the spectral peak) and faults of the study area. Yellow triangles show the location of the Sabalan Mountain and Sahand Mountain and blue circles indicate the hot springs.

DISCUSSION AND CONCLUSIONS

One of the most interesting and important locations for geothermal exploration is the Northwest of Iran, within which Sabalan geothermal field is located (Yousefi et al. 2010). In this study, spectral analysis was done to estimate the CPD, geothermal gradient and the heat flow on RTP aeromagnetic data. In the study area, the CPD obtained by using the centroid method, forward modeling spectral peak method and de-fractal method varied from 9.2 to 13.9 km, 8.9 to 13.7 km and 7.2 to 12.9 km, respectively. In addition, the heat flow values ranged from 16 to 104.3 mW/m², 105.8 to 162.9 mW/m² and 80.5 to 12.3 mW/m² as obtained by using the centroid method, forward modeling spectral peak method and de-fractal method, respectively.

In the applied methods, the lowest CPD value was estimated by the de-fractal method as the fractal property of magnetization was considered on the power spectrum. The ability to specify the range of fractal parameter is considered as an advantage of the de-fractal method. Moreover, this method can be used to estimate simultaneously the depth to the

bottom of the magnetic sources via the centroid method and forward modeling of the spectral peak method.

The results obtained based on the aforementioned methods indicated that regions A and B in the northwest of Iran (Fig. 18), especially Sabalan geothermal area (A), were highly promising areas for geothermal exploration. Moreover, hot springs were regarded as superficial evidence, corroborating the existence of subsurface geothermal resources in the study area (Yousefi et al. 2007; Noorollahi et al. 2009). Numerous hot springs, the temperature of which ranged from 45 to 86 °C, were spotted in different regions of the study area. These hot springs are the indicators of thermal activities occurring in depth (Fotouhi 1995). A good correlation was observed between the results of this study and the ones previously conducted in this area. In addition to Sabalan geothermal field, shallower CPDs, the depths of which were less than 9.4 km, appeared in region (B) “Kharajo”, which could be the result of crustal thinning. Furthermore, the shallower CPDs were created because of tectonic conditions and

Table 2. Estimated CPDs, geothermal gradients, heat-flow (forward modeling of the spectral peak)

Block number	Coordinates (UTM)		Z_t (km)	CPD (km)	Geothermal gradient ($^{\circ}\text{C}/\text{km}$)	Heat flow (mW/m^2)
	Easting (km)	Northing (km)				
1	689,950.3	4,050,000	3.8	11.9	48.7	121.8
2	729,950.3	4,050,000	1.9	11.6	50.0	125.0
3	769,950.3	4,050,000	3.7	10.8	53.7	134.3
4	809,950.3	4,050,000	2.6	11.8	49.2	122.9
5	569,950.3	4,090,000	2.1	10.1	57.4	143.6
6	609,950.3	4,090,000	1.4	9.3	62.4	155.9
7	649,950.3	4,090,000	2.8	12.6	46.0	115.1
8	689,950.3	4,090,000	4.9	10.1	46.4	116.0
9	729,950.3	4,090,000	1.5	10.4	55.8	139.4
10	769,950.3	4,090,000	2.1	10.3	56.3	140.8
11	809,950.3	4,090,000	1.9	11.4	50.9	127.2
12	849,950.3	4,090,000	1.2	9.9	58.6	146.5
13	569,950.3	4,130,000	1.5	9.4	61.7	154.3
14	609,950.3	4,130,000	2.9	11.6	50.0	125.0
15	649,950.3	4,130,000	1.6	12.1	47.9	119.8
16	689,950.3	4,130,000	4.2	11.1	52.3	130.6
17	729,950.3	4,130,000	3.8	10.1	57.4	143.6
18	769,950.3	4,130,000	3.4	12.3	47.2	117.9
19	809,950.3	4,130,000	1.2	13.3	43.6	109.0
20	849,950.3	4,130,000	2.6	11.6	50.0	125.0
21	529,950.3	4,170,000	3.1	9.1	63.7	159.3
22	569,950.3	4,170,000	2.9	9.8	59.2	148.0
23	609,950.3	4,170,000	5.2	10.3	56.3	140.8
24	649,950.3	4,170,000	2.4	12.8	45.3	113.3
25	689,950.3	4,170,000	4.1	13.1	44.3	110.7
26	729,950.3	4,170,000	3.2	13.4	43.3	108.2
27	769,950.3	4,170,000	1.6	12.1	47.9	119.8
28	809,950.3	4,170,000	1.8	9.5	61.1	152.6
29	849,950.3	4,170,000	2.1	9.3	62.4	155.9
30	889,950.3	4,170,000	3.8	12.2	47.5	118.9
31	529,950.3	4,210,000	4.1	10.3	56.3	140.8
32	569,950.3	4,210,000	1.3	11.6	50.0	125.0
33	609,950.3	4,210,000	2.9	10.7	54.2	135.5
34	649,950.3	4,210,000	3.6	10.3	56.3	140.8
35	689,950.3	4,210,000	2.3	9.7	59.8	149.5
36	729,950.3	4,210,000	1.1	9.1	63.7	159.3
37	769,950.3	4,210,000	0.8	8.9	65.2	162.9
38	809,950.3	4210000	3.1	10.2	56.9	142.2
39	849,950.3	4,210,000	4.2	10.3	56.3	140.8
40	529,950.3	4,250,000	3.3	10.9	53.2	133.0
41	569,950.3	4,250,000	3.9	12.1	47.9	119.8
42	609,950.3	4,250,000	4.2	13.2	43.9	109.8
43	649,950.3	4,250,000	4.9	11.9	46.8	116.9
44	689,950.3	4,250,000	5.3	12.6	46.0	115.1
45	729,950.3	4,250,000	4.9	9.5	61.1	152.6
46	769,950.3	4,250,000	5.1	9.3	62.4	155.9
47	809,950.3	4,250,000	6.1	10.0	58.0	145.0
48	849,950.3	4,250,000	4.9	11.4	50.9	127.2
49	529,950.3	4,290,000	4.7	12.9	45.0	112.4
50	569,950.3	4,290,000	5.4	13.7	42.3	105.8
51	609,950.3	4,290,000	5.3	13.1	44.3	110.7
52	649,950.3	4,290,000	2.9	11.8	49.2	122.9
53	689,950.3	4,290,000	3.1	10.7	54.2	135.5
54	729,950.3	4,290,000	2.8	9.4	58.6	146.5
55	769,950.3	4,290,000	5.8	13.2	43.9	109.8

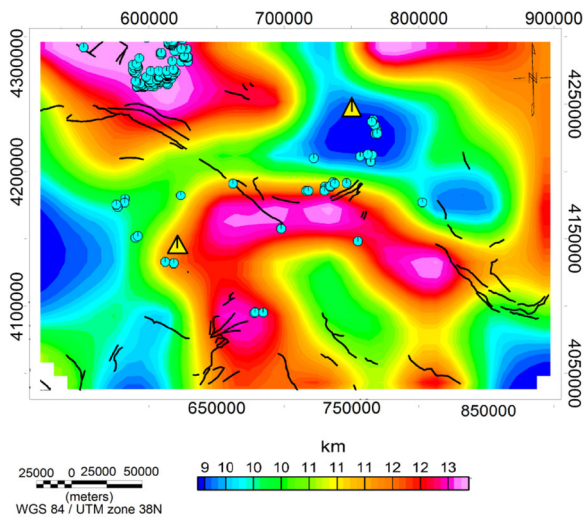


Figure 14. Measured power spectrum (green dotted line) and the result of forward-modeling (red line). The depth to the top is: (a) $Z_1 = 4.9$ km, and $Z_0 = 10.1$ km for block 8; (b) $Z_1 = 5.2$ km, and $Z_0 = 10.3$ km for the block 23; (c) $Z_1 = 5.3$ km and $Z_0 = 12.6$ km for block 44.

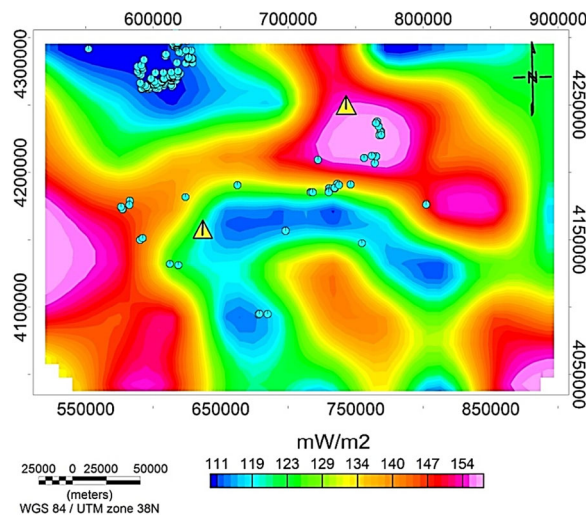


Figure 16. Heat-flow map (forward modeling of the spectral peak) of the study area. Yellow triangles show the location of the Sabalan Mountain and Sahand Mountain and blue circles show hot springs.

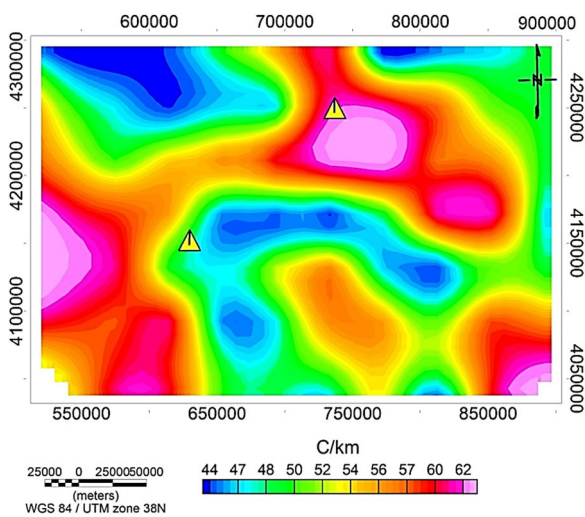


Figure 15. Geothermal gradient map (forward modeling of the spectral peak) of the study area. Yellow triangles show the location of the Sabalan Mountain and Sahand Mt.

earthquake distributions of the depth in the A and B regions.

In the present research, the Curie depth results were in good agreement with the well data in the Sabalan geothermal site. The results of this study can be conducive to finding probable geothermal reservoirs in the region, only if the shallow CDPs are properly correlated with the depth and density of

earthquakes, geothermal anomalies, and tectonic regime.

The amplitude changes of total magnetic intensity can be employed for the unknown igneous bodies, especially those emplaced within sedimentary rocks. Magnetic anomalies are commonly associated with the type of basement (igneous and/or metamorphic) rocks, lava flows, intrusive plugs, volcanic rocks and generally igneous bodies within sedimentary columns. The depth of the magnetic basement is relatively shallow in Sabalan volcanic area, particularly in the east of the dome. Sabalan geothermal field is considered as one of the most promising geothermal hydrothermal fields for geothermal exploration in Iran owing to the existence of myriad hot springs (Teknik and Ghods 2017).

Given the previous definition of the CPD, the minimum CPD for different areas is known as the indicator of a warmer block (low CPD) compared to the adjacent areas. Teknik and Ghods (2017) produced a “depth of magnetic basement” map (DMB) of Iran, the results of which indicated that DMB was in the range of 2–7 km in the study area. Moreover, these two areas, having different curie depths, were separated by the main faults, almost extended between the two areas with lower and higher curie depths (Fig. 18).

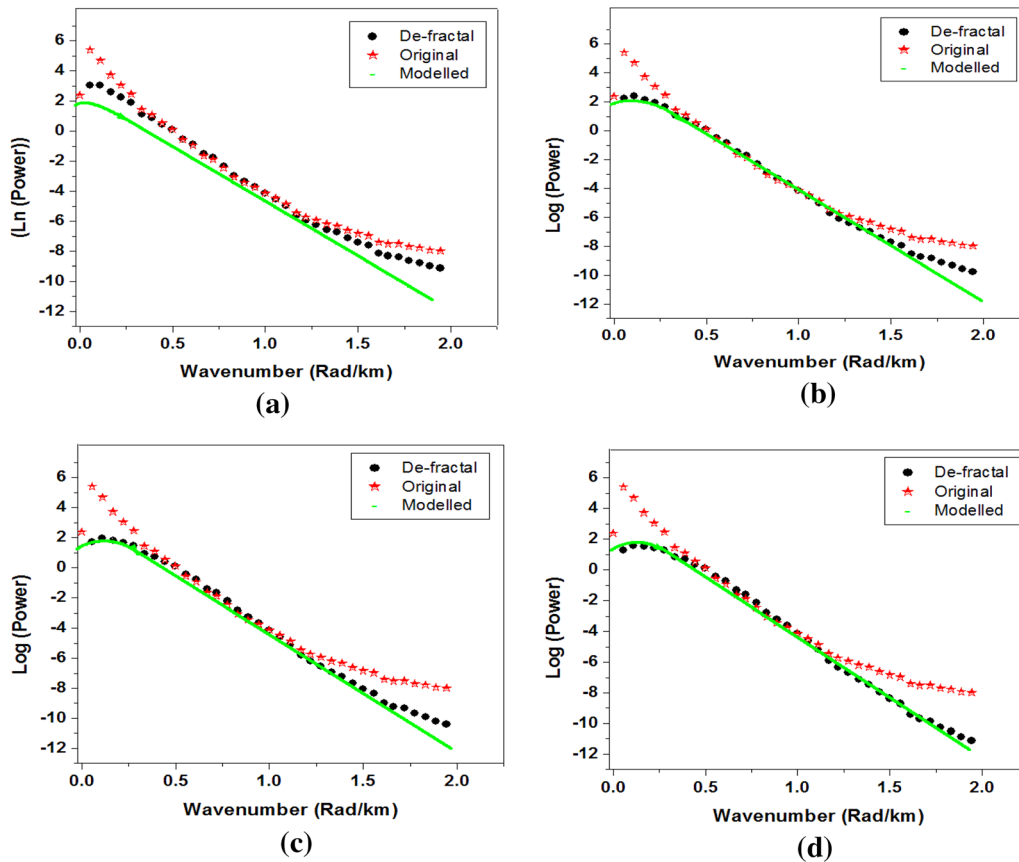


Figure 17. Comparison of de-fractal power spectra for block 40 using different α values (a) 1; (b) 2; (c) 3; (d) 3.3 and modeled curves, produced by using the best fitting of estimated parameters.

In this study, the results of Curie depth indicated that the frequency of earthquakes in an area is associated with the CPD (Fig. 18).

Since earthquake occurrence is dependent on the temperature variation of blocks, a specific temperature range can be assigned to the possibility of earthquake occurrences, hence the conclusion that a significant conformity exists between earthquake records and the estimated curie depth. An example would be the Sabalan geothermal area, which has a low CPD and is adjacent to a high CPD area with high earthquake records. Generally, it can be concluded that earthquakes mainly occur in the border of warm and cold blocks. Areas with high geothermal potential can be recognized by integrating the geological, geochemical and geophysical information.

As previously mentioned, the shallow Curie point can be regarded as a favorable geothermal reservoir when associated with other fundamental parameters such as suitable structures and permeabilities. Mountain, with a CPD of less than 8.5 km and a heat flow range of more than 135 mW/m².

This area is comprised of two specified zones with CPD of less than 7.5 km and heat flow rates of more than 155 mW/m². Several exploratory wells, shown in Figure 19, have been investigated for temperature logs at a stable situation in Sabalan geothermal field (Porkhial et al. 2015).

Well NWS8 has been drilled to a vertical depth of 2270 m, and unlike other wells, it has not been affected by thermal convection processes in the reservoir. The temperature log of NWS8, demonstrated in Figure 19b, could be described as an

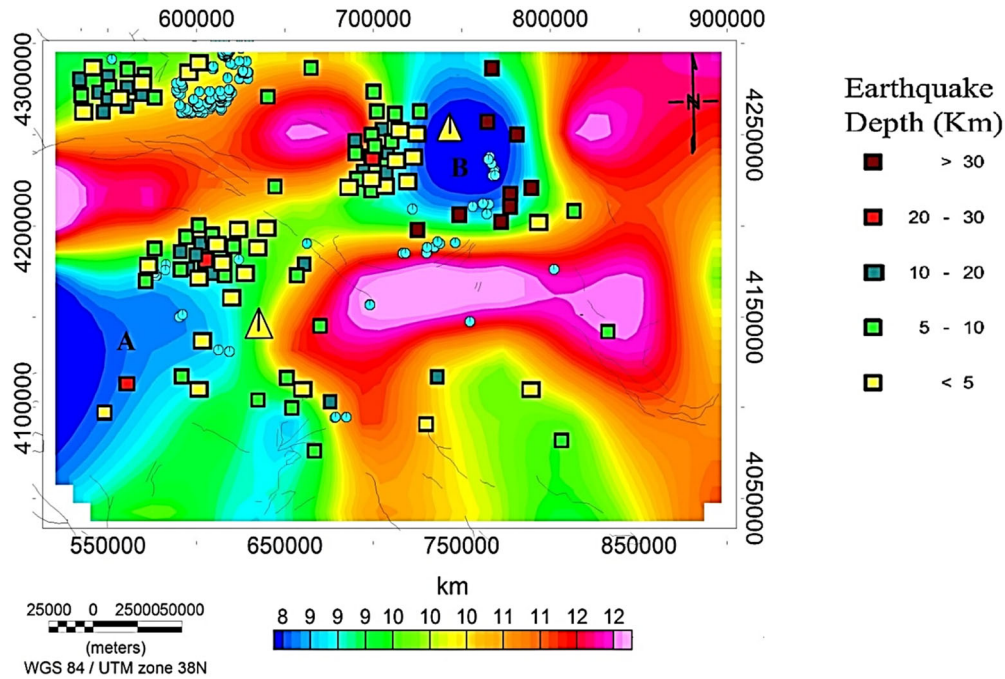


Figure 18. CPD map for a de-fractal method and earthquake distribution in the study area. The yellow triangles are Sabalan Mountain and Sahand Mountain and the blue circles show hot springs.

increasing function of depth to determine the thermal gradient, which is $0.0901\text{ }^{\circ}\text{C/m}$.

CPD in the well NWS8 will be 6.44 km, which is approximately consistent with the estimated results obtained by the de-fractal method. Although other regions introduced in this study, including the shallowest curie points, were correlated with other geothermal evidence such as accurate structures and hot springs of the region, more precise information is to be obtained by conducting studies on drilling wells and geochemical and geophysical data. However, it is to be noted that only one well can be used due to the strong convection effects in all other wells, which clearly affect the geothermal gradient in the whole area. It should also be noted that convection might increase isotherms as observed from the well logs, where a temperature of approximately $240\text{ }^{\circ}\text{C}$ occurred at depths of 3 km to almost 1 km due to more efficient heat transport by convection.

Magneto-telluric (MT) soundings, selected from 50 stations, were conducted by SKM in 1998 and obtained through the resistivity contours of the inversion of the magneto-telluric data. Figure 21b shows the temperature contours on the geological section, created using three exploration wells and two shallow injection wells. As shown in Figure 20,

the heat flow value of the geothermal resource, obtained from the de-fractal method, was placed in the range of $174\text{--}204.2\text{ mW/m}^2$, which was higher than the values of the centroid and forward modeling spectral peak methods. As shown in Table 4, the maximum temperature belonged to NWS1 well. As shown in Figure 21, a low resistivity anomaly area (less than 10 ohm-m) beneath well NWS1 was properly correlated with CPDs, derived from the de-fractal method. Figure 22 shows the hydro-electrical model and the conceptual model of heat flow movement in the northwest of Sablan, obtained through magnetotelluric and wells data.

Power spectrum curve is the nature and features of magnetic field intensity of the block; moreover, it is known that different geology units present various magnetic responses based on their type and material. Since the present study area covers a larger extent, it contains a greater variety of geology units, hence the different responses expected from magnetic field intensity (as an effective factor on power spectrum curve). Generally, the factor determining fractal parameter amount is the type of rocks and geology units. Therefore, by removing the magnetization fractal property from power spectrum curve in different depths and wavelengths, the slope of the

Table 3. Results of the estimation of the depth to the top and bottom of the magnetic layer

Block number	Coordinates (UTM)		Z_t (km)	CPD (km)	Geothermal gradient ($^{\circ}\text{C}/\text{km}$)	Heat flow (mW/m)	Fractal index
	Easting (km)	Northing (km)					
1	689,950.3	4,050,000	2.8	10.6	54.7	136.8	3.4
2	729,950.3	4,050,000	3.1	10.5	55.2	138.1	2.3
3	769,950.3	4,050,000	2.5	10.1	57.4	143.6	2.8
4	809,950.3	4,050,000	2.7	9.8	59.2	148.0	2.2
5	569,950.3	4,090,000	2.8	8.9	65.2	162.9	2.5
6	609,950.3	4,090,000	1.6	9.8	59.2	148.0	2.4
7	649,950.3	4,090,000	2.7	8.4	69.0	172.6	3.0
8	689,950.3	4,090,000	1.9	11.2	51.8	129.5	2.9
9	729,950.3	4,090,000	2.5	10.6	54.7	136.8	2.6
10	769,950.3	4,090,000	1.7	10.1	57.4	143.6	2.4
11	809,950.3	4,090,000	1.5	9.8	59.2	148.0	2.7
12	849,950.3	4,090,000	2.8	10.9	53.2	133.0	3.1
13	569,950.3	4,130,000	1.9	8.4	69.0	172.6	2.3
14	609,950.3	4,130,000	2.5	8.6	67.4	168.6	2.4
15	649,950.3	4,130,000	1.5	11.1	52.3	130.6	2.5
16	689,950.3	4,130,000	1.2	11.6	50.0	125.0	2.8
17	729,950.3	4,130,000	0.7	10.7	54.2	135.5	2.1
18	769,950.3	4,130,000	0.7	10.1	57.4	143.6	2.2
19	809,950.3	4,130,000	1.9	11.4	50.9	127.2	2.1
20	849,950.3	4,130,000	1.5	11.9	48.7	121.8	2.7
21	529,950.3	4,170,000	1.8	8.3	69.9	174.7	2.4
22	569,950.3	4,170,000	2.1	8.5	68.2	170.6	2.3
23	609,950.3	4,170,000	1.9	9.1	63.7	159.3	2.1
24	649,950.3	4,170,000	2.5	10.1	57.4	143.6	2.2
25	689,950.3	4,170,000	2.9	12.1	47.9	119.8	2.7
26	729,950.3	4,170,000	1.8	12.9	45.0	112.4	2.8
27	769,950.3	4,170,000	2.3	12.7	45.7	114.2	2.4
28	809,950.3	4,170,000	1.0	11.9	48.7	121.8	2.6
29	849,950.3	4,170,000	0.9	12.1	47.9	119.8	3.1
30	889,950.3	4,170,000	1.4	10.1	57.4	143.6	2.3
31	529,950.3	4,210,000	1.7	12.8	45.3	113.3	2.8
32	569,950.3	4,210,000	2.1	11.9	48.7	121.8	2.4
33	609,950.3	4,210,000	2.3	10.7	54.2	135.5	2.5
34	649,950.3	4,210,000	2.2	10.1	57.4	143.6	3.0
35	689,950.3	4,210,000	1.6	9.4	61.7	154.3	2.1
36	729,950.3	4,210,000	1.1	8.6	67.4	168.6	2.3
37	769,950.3	4,210,000	0.8	8.3	69.9	174.7	2.2
38	809,950.3	4,210,000	1.5	10.3	56.3	140.8	2.3
39	849,950.3	4,210,000	1.9	11.2	51.8	129.5	2.1
40	529,950.3	4,250,000	1.7	10.5	55.2	138.1	2.0
41	569,950.3	4,250,000	1.5	10.8	53.7	134.3	2.4
42	609,950.3	4,250,000	1.6	11.0	52.7	131.8	2.7
43	649,950.3	4,250,000	1.2	12.1	47.9	119.8	3.1
44	689,950.3	4,250,000	0.9	11.9	48.7	121.8	2.6
45	729,950.3	4,250,000	2.1	7.6	76.3	190.8	2.7
46	769,950.3	4,250,000	1.4	7.1	81.7	204.2	2.4
47	809,950.3	4,250,000	1.4	11.9	48.7	121.8	2.6
48	849,950.3	4,250,000	0.9	11.7	49.6	123.9	2.2
49	529,950.3	4,290,000	2.3	9.4	61.7	154.3	2.1
50	569,950.3	4,290,000	2.5	9.8	59.2	148.0	3.1
51	609,950.3	4,290,000	2.9	10.1	57.4	143.6	3.3
52	649,950.3	4,290,000	1.8	10.4	55.8	139.4	2.9
53	689,950.3	4,290,000	2.3	10.3	56.3	140.8	2.7
54	729,950.3	4,290,000	1.3	8.9	65.2	162.9	2.2
55	769,950.3	4,290,000	2.5	9.3	62.4	155.9	2.1

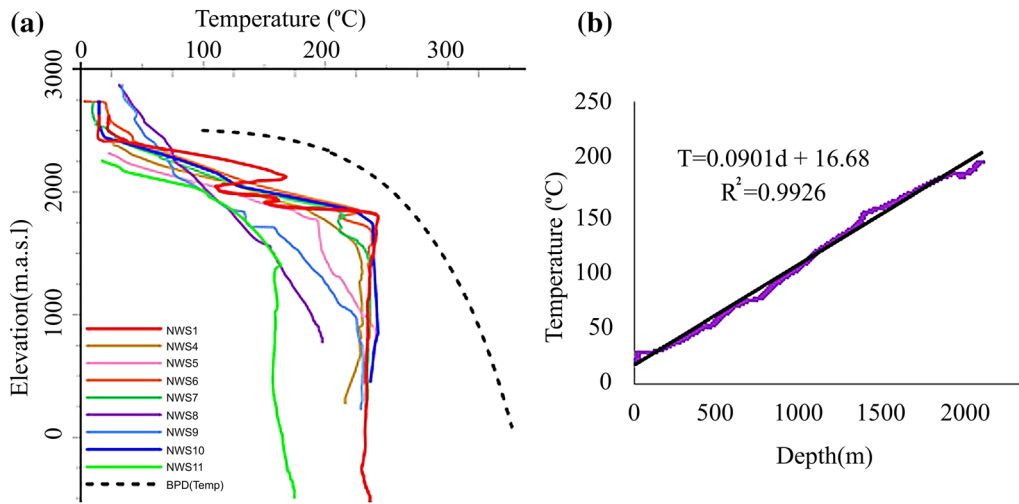


Figure 19. (a) Wells steady-state temperature logs in the Sabalan geothermal field (Porkhial et al. 2015). (b) Thermal gradient in well NWS8.

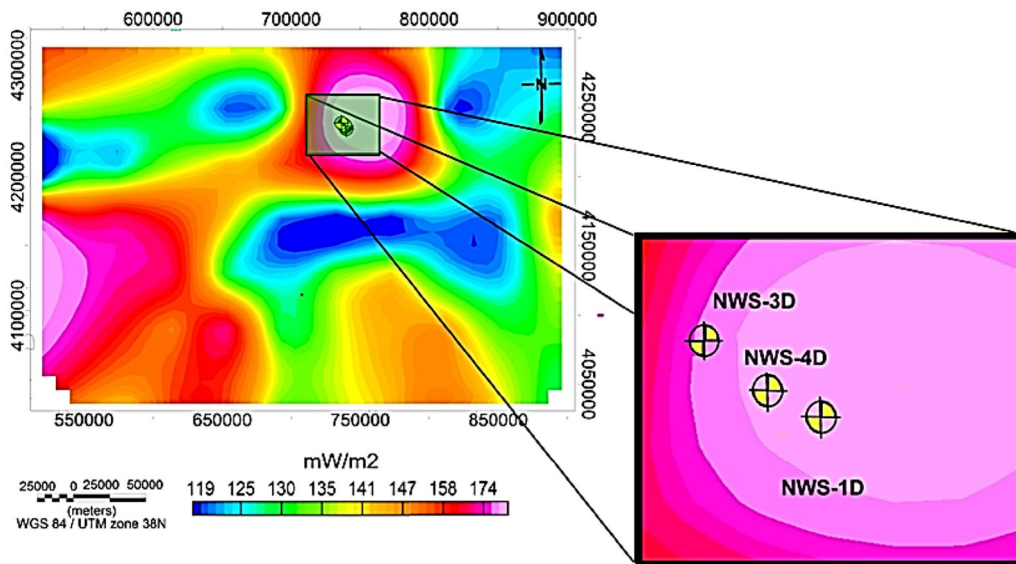


Fig. 20. Wells location on the heat flow map, derived from the de-fractal method.

power spectrum curve is expected to decrease in different amounts. As shown in Figure 17, the amount of fractal parameter in different wavelengths on power spectrum curve (block 40) is not high and removing its fractal property does not significantly reduce the slope of the power spectrum curve. Therefore, the value of fractal parameter for all blocks and different areas does not follow a

similar pattern but depends on the geological features and responses of magnetic field intensity. Figure 17 shows the process of selecting an optimal amount of fractal index; by increasing the fractal parameters amounts, the curve does not experience a significant slope reduction due to the geological features and selection of a block with the least fractal properties. As a result, no significant slope

Table 4. Specifications of three exploration wells (Noorollahi et al. 2009)

Well	NWS1	NWS3	NWS4
Location (UTM)	739108 E 4238580 N	737028 E 4240784 N	738712 E 4239833 N
Elevation (m a.s.l)	2632	2277	2487
Well depth (m)	3197	3177	2266
Well permeable zones (m a.s.l)	1800–1400 200–0 – 200 to 350	No permeable zone	1050–900 880–890
Maximum temperature (8 °C)	240	148	229

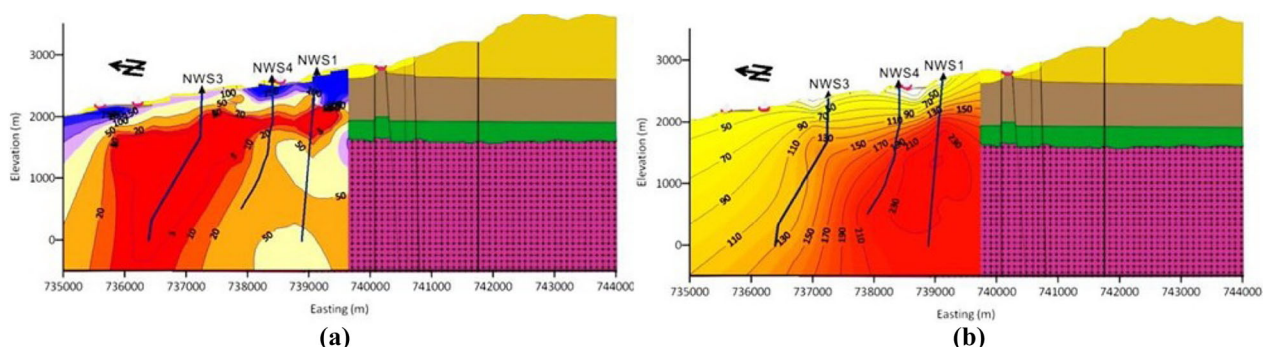


Figure 21. (a) Resistivity distribution in the northwest of Sabalan Mountain (resistivity in Ohm m); (b) temperature contours in the northwest of Sabalan Mountain (T in °C) (Noorollahi and Itoi 2011).

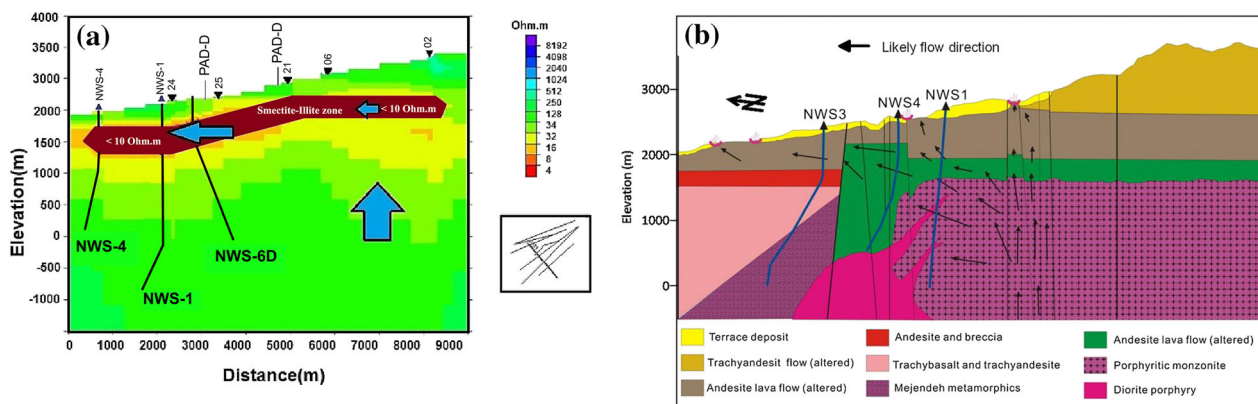


Figure 22. (a) Postulated a hydro-electrical model of the North–West Sabalan geothermal field (Porkhial et al. 2001); (b) a conceptual model of the NW Sabalan geothermal field (Noorollahi and Itoi 2011).

reduction was observed in different wavelengths of de-fractal spectrum. Figure 23 shows the process of best fitting to choose the most optimal value of fractal parameter for blocks 43 and 51. Because these blocks have high fractal parameter value,

removing the fractal effect and de-fractal power spectrum curve considerably reduce slope of the power spectrum curve and the process of making power spectrum curve horizontal due to the increase in the value of fractal parameter.

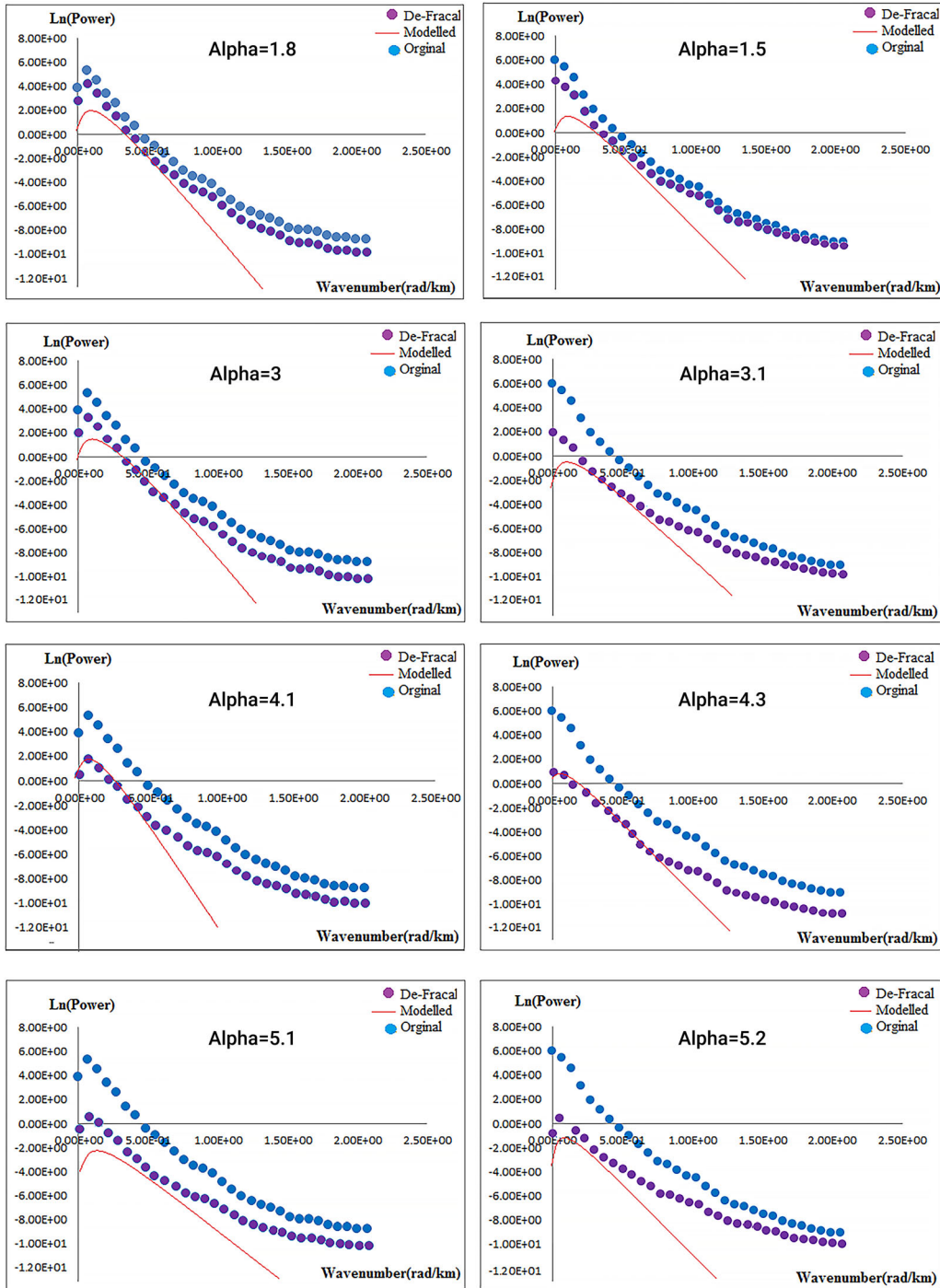


Figure 23. Process of the best fitting for choose the most optimal amount for fractal parameter ((a) Block 43; (b) Block 51).

REFERENCES

- Aboud, E., Salem, A., & Mekkawi, M. (2011). Curie depth map for Sinai Peninsula, Egypt deduced from the analysis of magnetic data. *Tectonophysics*, 506(1), 46–54.
- Afshar, A., Norouzi, G. H., Moradzadeh, A., Riahi, M. A., & Porkhial, S. (2017). Curie point depth, geothermal gradient and heat-flow estimation and geothermal anomaly exploration from integrated analysis of aeromagnetic and gravity data on the Sabalan area, NW Iran. *Pure and Applied Geophysics*, 174(3), 1133–1152.
- Akbar, S., & Fathianpour, N. (2016). Improving the Curie depth estimation through optimizing the spectral block dimensions of the aeromagnetic data in the Sabalan geothermal field. *Journal of Applied Geophysics*, 135, 281–287.
- Amirpour-Asl, A., Ghods, A., Rezaeian, M., & Bahroudi, A. (2010). Depth of curie temperature isotherm from aeromagnetic spectra in Iran: Tectonics implications. In *Tectonic crossroads: Evolving orogens of Eurasia-Africa-Arabia*, Ankara, Turkey, Geological Society of America International Section, Abstracts with Program (Vol. 65).
- Aydın, I., & Oksum, E. (2010). Exponential approach to estimate the Curie-temperature depth. *Journal of Geophysics and Engineering*, 7(2), 113.
- Azad, S. S., Dominguez, S., Philip, H., Hessami, K., Forutan, M. R., Zadeh, M. S., et al. (2011). The Zandjan fault system: Morphological and tectonic evidence of a new active fault network in the NW of Iran. *Tectonophysics*, 506(1–4), 73–85.
- Bansal, A. R., & Dimri, V. P. (1999). Gravity evidence for mid crustal domal structure below Delhi fold belt and Bhilwara super group of western India. *Geophysical Research Letters*, 26(18), 2793–2795.
- Bansal, A. R., & Dimri, V. P. (2001). Depth estimation from the scaling power spectral density of nonstationary gravity profile. *Pure and Applied Geophysics*, 158(4), 799–812.
- Bansal, A. R., Dimri, V. P., Kumar, R., & Anand, S. P. (2016). Curie depth estimation from aeromagnetic for fractal distribution of sources. In V. P. Dimri (Ed.), *Fractal solutions for understanding complex systems in earth sciences* (pp. 19–31). Cham: Springer.
- Bansal, A. R., Dimri, V. P., & Sagar, G. V. (2006). Quantitative interpretation of gravity and magnetic data over southern granulite terrain using scaling spectral approach. *Journal-Geological Society of India*, 67(4), 469.
- Bansal, A. R., Gabriel, G., & Dimri, V. P. (2010). Power law distribution of susceptibility and density and its relation to seismic properties: An example from the German Continental Deep Drilling Program (KTB). *Journal of Applied Geophysics*, 72(2), 123–128.
- Bansal, A. R., Gabriel, G., Dimri, V. P., & Krawczyk, C. M. (2011). Estimation of depth to the bottom of magnetic sources by a modified centroid method for fractal distribution of sources: An application to aeromagnetic data in Germany. *Geophysics*, 76(3), L11–L22.
- Bédard, Karine, Comeau, Félix-Antoine, Raymond, Jasmin, Malo, Michel, & Nasr, Maher. (2018). Geothermal characterization of the St. Lawrence Lowlands sedimentary basin, Québec, Canada. *Natural Resources Research*, 27(4), 479–502. <https://doi.org/10.1007/s11053-017-9363-2>.
- Bhattacharyya, B. K., & Leu, L. K. (1977). Spectral analysis of gravity and magnetic anomalies due to rectangular prismatic bodies. *Geophysics*, 42(1), 41–50.
- Bilim, F., Akay, T., Aydemir, A., & Kosaroglu, S. (2016). Curie point depth, heat-flow and radiogenic heat production deduced from the spectral analysis of the aeromagnetic data for geothermal investigation on the Menderes Massif and the Aegean Region, western Turkey. *Geothermics*, 60, 44–57.
- Blakely, R. J. (1988). Curie temperature isotherm analysis and tectonic implications of aeromagnetic data from Nevada. *Journal of Geophysical Research: Solid Earth*, 93(B10), 11817–11832.
- Blakely, R. J. (1996). *Potential theory in gravity and magnetic applications*. Cambridge: Cambridge University Press.
- Bogie, I., Cartwright, A. J., Khosrawi, K., Talebi, B., & Sahabi, F. (2000). The Meshkin Shahr geothermal prospect, Iran. In *Proceedings of the world geothermal congress 2000*, Kyushu-Tohoku, Japan (pp. 997–1002).
- Bouligand, C., Glen, J. M., & Blakely, R. J. (2009). Mapping Curie temperature depth in the western United States with a fractal model for crustal magnetization. *Journal of Geophysical Research: Solid Earth*, 114(B11), 1–25.
- Bromley, C., Khosrawi, K., & Talebi, B. (2000). Geophysical exploration of Sabalan geothermal prospects in Iran. In *Proceedings of the world geothermal congress*, Japan.
- Connard, G., Couch, R., & Gemperle, M. (1983). Analysis of aeromagnetic measurements from the Cascade Range in central Oregon. *Geophysics*, 48(3), 376–390.
- Dimri, V. P., Bansal, A. R., Srivastava, R. P., & Vedanti, N. (2003). Scaling behaviour of real earth source distribution: Indian Case Studies. In T. M. Mahadevan, B. R. Arora, & K. R. Gupta (Eds.), *Indian continental lithosphere: Emerging research trends, memoir geological society of India* (Vol. 53, pp. 431–448).
- Fedi, M., Quarta, T., & De Santis, A. (1997). Inherent power-law behavior of magnetic field power spectra from a sector and grant ensemble. *Geophysics*, 62(4), 1143–1150.
- Finn, C. A., & Ravat, D. (2004). Magnetic depth estimates and their potential for constraining crustal composition and heat flow in Antarctica. In *AGU fall meeting abstracts*.
- Fotouhi, M. (1995). Geothermal development in Sabalan, Iran. In *Proceedings of the world geothermal congress 1995*, Florence, Italy (Vol. 1, pp. 191–196).
- Ghaedrahmati, R., Moradzadeh, A., Fathianpour, N., Lee, S. K., & Porkhial, S. (2013). 3-D inversion of MT data from the Sabalan geothermal field, Ardabil, Iran. *Journal of Applied Geophysics*, 93, 12–24.
- Hsieh, H. H., Chen, C. H., Lin, P. Y., & Yen, H. Y. (2014). Curie point depth from spectral analysis of magnetic data in Taiwan. *Journal of Asian Earth Sciences*, 90, 26–33.
- Khojamli, A., Ardejani, F. D., Moradzadeh, A., Kalate, A. N., Kahoo, A. R., & Porkhial, S. (2016). Estimation of Curie point depths and heat flow from Ardebil province, Iran, using aeromagnetic data. *Arabian Journal of Geosciences*, 9(5), 383.
- Khojamli, A., Doulati Ardejani, F., Moradzadeh, A., Nejati Kalateh, A., Roshandel Kahoo, A., & Porkhial, S. (2017). Determining fractal parameter and depth of magnetic sources for Ardabil geothermal area using aeromagnetic data by de-fractal approach. *Journal of Mining and Environment*, 8(1), 93–101.
- Khosrawi, K. (2008). The geothermal resource in Sabalan, Iran. In *Geothermal training programme, 30th anniversary workshop*, United Nations University, August.
- Kiyak, A., Karavul, C., Gülen, L., Peksen, E., & Kiliç, A. R. (2015). Assessment of geothermal energy potential by geophysical methods: Nevşehir Region, Central Anatolia. *Journal of Volcanology and Geothermal Research*, 295, 55–64.
- KML. (1998). *Sabalan geothermal project, stage 1-surface exploration, final exploration report*. Report number 2505-RPT-GE-003.
- Maden, N. (2010). Curie-point depth from spectral analysis of magnetic data in Erciyes stratovolcano (Central Turkey). *Pure and Applied Geophysics*, 167(3), 349–358.
- Maus, S., & Dimri, V. P. (1994). Scaling properties of potential fields due to scaling sources. *Geophysical Research Letters*, 21(10), 891–894.

- Maus, S., & Dimri, V. (1995). Potential field power spectrum inversion for scaling geology. *Journal of Geophysical Research: Solid Earth*, 100(B7), 12605–12616.
- Maus, S., Gordon, D., & Fairhead, D. (1997). Curie-temperature depth estimation using a self-similar magnetization model. *Geophysical Journal International*, 129(1), 163–168.
- McKenzie, D. (1972). Active tectonics of the Mediterranean region. *Geophysical Journal International*, 30(2), 109–185.
- Noorollahi, Younes, Bina, Saeid Mohammadzadeh, & Yousefi, Hossein. (2016). Simulation of power production from dry geothermal well using down-hole heat exchanger in Sabalan field, Northwest Iran. *Natural Resources Research*, 25(2), 227–239. <https://doi.org/10.1007/s11053-015-9270-3>.
- Noorollahi, Y., & Itoi, R. (2011). Production capacity estimation by reservoir numerical simulation of northwest (NW) Sabalan geothermal field, Iran. *Energy*, 36(7), 4552–4569.
- Noorollahi, Y., Itoi, R., Fujii, H., & Tanaka, T. (2008). GIS integration model for geothermal exploration and well siting. *Geothermics*, 37(2), 107–131.
- Noorollahi, Y., Yousefi, H., Itoi, R., & Ehara, S. (2009). Geothermal energy resources and development in Iran. *Renewable and Sustainable Energy Reviews*, 13(5), 1127–1132.
- Nwankwo, L. I., & Shehu, A. T. (2015). Evaluation of Curie-point depths, geothermal gradients and near-surface heat flow from high-resolution aeromagnetic (HRAM) data of the entire Sokoto Basin, Nigeria. *Journal of Volcanology and Geothermal Research*, 305, 45–55.
- Obande, G. E., Lawal, K. M., & Ahmed, L. A. (2014). Spectral analysis of aeromagnetic data for geothermal investigation of Wikki Warm Spring, north-east Nigeria. *Geothermics*, 50, 85–90.
- Okubo, Y., Graf, R. J., Hansen, R. O., Ogawa, K., & Tsu, H. (1985). Curie point depths of the island of Kyushu and surrounding areas, Japan. *Geophysics*, 50(3), 481–494.
- Pilkington, M., & Todoeschuck, J. P. (1993). The fractal magnetization of continental crust. *Geophysical Research Letters*, 20, 627–630.
- Porkhial, S., Abdollahzadeh Bina, F., Radmehr, B., & Johari Sefid, P. (2015). Interpretation of the injection and heat up tests at Sabalan geothermal field, Iran. In *Proceedings world geothermal congress* (pp. 19–25).
- Porkhial, S., Ghomshei, M. M., & Yousefi, P. (2001). Geothermal energy in Iran. *Weather*, 2002, 431–448.
- Porwal, A., Carranza, E. J. M., & Hale, M. (2003). Knowledge-driven and data-driven fuzzy models for predictive mineral potential mapping. *Natural Resources Research*, 12(1), 1–25.
- Porwal, A., Carranza, E. J. M., & Hale, M. (2006). A hybrid fuzzy weights-of-evidence model for mineral potential mapping. *Natural Resources Research*, 15(1), 1–14. <https://doi.org/10.1007/s11053-006-9012-7>.
- Rao, C. R., Kishore, R. K., Kumar, V. P., & Babu, B. B. (2011). Delineation of intra crustal horizon in Eastern Dharwar Craton—An aeromagnetic evidence. *Journal of Asian Earth Sciences*, 40(2), 534–541.
- Ravat, D., Pignatelli, A., Nicolosi, I., & Chiappini, M. (2007). A study of spectral methods of estimating the depth to the bottom of magnetic sources from near-surface magnetic anomaly data. *Geophysical Journal International*, 169(2), 421–434.
- Rebai, A., & Goffinet, B. (1993). Power of tests for QTL detection using replicated progenies derived from a diallel cross. *Theoretical and Applied Genetics*, 86(8), 1014–1022.
- Ross, H. E., Blakely, R. J., & Zoback, M. D. (2006). Testing the use of aeromagnetic data for the determination of Curie depth in California. *Geophysics*, 71(5), L51–L59.
- Saibi, H., Aboud, E., & Gottsmann, J. (2015). Curie point depth from spectral analysis of aeromagnetic data for geothermal reconnaissance in Afghanistan. *Journal of African Earth Sciences*, 111, 92–99.
- Salem, A., Green, C., Ravat, D., Singh, K. H., East, P., Fairhead, J. D., et al. (2014). Depth to Curie temperature across the central Red Sea from magnetic data using the de-fractal method. *Tectonophysics*, 624, 75–86.
- Salem, A., Ushijima, K., Elsirafi, A., & Mizunaga, H. (2000). Spectral analysis of aeromagnetic data for geothermal reconnaissance of Quseir area, northern Red Sea, Egypt. In *Proceedings of the world geothermal congress* (Vol. 16691674).
- Shuey, R. T., Schellinger, D. K., Tripp, A. C., & Alley, L. B. (1977). Curie depth determination from aeromagnetic spectra. *Geophysical Journal International*, 50(1), 75–101.
- Spector, A., & Grant, F. S. (1970). Statistical models for interpreting aeromagnetic data. *Geophysics*, 35(2), 293–302.
- Stampolidis, A., Kane, I., Tsokas, G. N., & Tsourlos, P. (2005). Curie point depths of Albania inferred from ground total field magnetic data. *Surveys in Geophysics*, 26(4), 461–480.
- Starostenko, V. I., Dolmaz, M. N., Kutas, R. I., Rusakov, O. M., Oksum, E., Hisarli, Z. M., et al. (2014). Thermal structure of the crust in the Black Sea: Comparative analysis of magnetic and heat flow data. *Marine Geophysical Research*, 35(4), 345–359. (**Suppl., Abstract T11A-1236**).
- Tanaka, A., Okubo, Y., & Matsubayashi, O. (1999). Curie point depth based on spectrum analysis of the magnetic anomaly data in East and Southeast Asia. *Tectonophysics*, 306(3), 461–470.
- Teknik, V., & Ghods, A. (2017). Depth of magnetic basement in Iran based on fractal spectral analysis of aeromagnetic data. *Geophysical Journal International*, 209(3), 1878–1891.
- Trifonova, P., Zhelev, Z., Petrova, T., & Bojadgieva, K. (2009). Curie point depths of Bulgarian territory inferred from geomagnetic observations and its correlation with regional thermal structure and seismicity. *Tectonophysics*, 473(3–4), 362–374.
- Waples, Douglas W. (2002). A new model for heat flow in extensional basins: Estimating radiogenic heat production. *Natural Resources Research*, 11(2), 125–133. <https://doi.org/10.1023/A:1015568119996>.
- Yousefi, H., Ehara, S., & Noorollahi, Y. (2007). Geothermal potential site selection using GIS in Iran. In *Proceedings of the 32nd workshop on geothermal reservoir engineering*, Stanford University, Stanford, California (pp. 174–182).
- Yousefi, H., Noorollahi, Y., Ehara, S., Itoi, R., Yousefi, A., Fujimitsu, Y., et al. (2010). Developing the geothermal resources map of Iran. *Geothermics*, 39(2), 140–151.